MULTISCALE MODEL. SIMUL.
Vol. 12, No. 2, pp. 832–878

PARAXIAL COUPLING OF PROPAGATING MODES IN THREE-DIMENSIONAL WAVEGUIDES WITH RANDOM BOUNDARIES*

LILIANA BORCEA† AND JOSSELIN GARNIER‡

Abstract. We analyze long range wave propagation in three-dimensional random waveguides. The waves are trapped by top and bottom boundaries, but the medium is unbounded in the two remaining directions. We consider scalar waves, and motivated by applications in underwater acoustics, we take a pressure release boundary condition at the top surface and a rigid bottom boundary. The wave speed in the waveguide is known, but the top boundary has small random fluctuations that cause significant cumulative scattering of the waves over long distances of propagation. To quantify the scattering effects, we study the evolution of the random amplitudes of the waveguide modes. We obtain that in the long range limit they satisfy a system of paraxial equations driven by a Brownian field. We use this system to estimate three important mode-dependent scales: the scattering mean free path, the cross-range decoherence length, and the decoherence frequency. Understanding these scales is important in imaging and communication problems, because they encode the cumulative scattering effects in the wave field measured by remote sensors. As an application of the theory, we analyze time reversal and coherent interferometric imaging in strong cumulative scattering regimes.

Key words. waveguides, random media, asymptotic analysis

AMS subject classifications. 76B15, 35Q99, 60F05

DOI. 10.1137/12089747X

1. Introduction.

We study long range scalar (acoustic) wave propagation in a three-dimensional waveguide. The setup is illustrated in Figure 1, and it is motivated by problems in underwater acoustics. We denote by $z \in \mathbb{R}$ the range, the main direction of propagation of the waves. The medium is unbounded in the cross-range direction $x \in \mathbb{R}$, but it is confined in depth y by two boundaries which trap the waves, thus creating the waveguide effect.

The acoustic pressure field is denoted by $p(t,x,y,z)$, and it satisfies the wave equation

$$\left[\partial_x^2+\partial_y^2+\partial_z^2-\frac{1}{c^2(y)}\partial_t^2\right]p(t,x,y,z) = f(t,x,y)\delta(z), \quad y \in [0,T(x,z)],\ x,z \in \mathbb{R},\ t>0, \tag{1.1}$$

in a medium with wave speed $c(y)$. The excitation is due to a source located in the plane $z=0$, emitting the pulse $f(t,x,y)$. The medium is quiescent before the source excitation,

$$p(t,x,y,z) = 0, \quad t \ll 0. \tag{1.2}$$

*Received by the editors November 2, 2012; accepted for publication (in revised form) April 9, 2014; published electronically June 24, 2014.
http://www.siam.org/journals/mms/12-2/89747.html

†Department of Mathematics, University of Michigan, Ann Arbor, MI 48109-1043 (borcea@umich.edu). This author's work was partially supported by AFSOR grant FA9550-12-1-0117, ONR grants N00014-12-1-0256, N00014-09-1-0290, and N00014-05-1-0699, and NSF grants DMS-0907746 and DMS-0934594.

‡Laboratoire de Probabilités et Modèles Aléatoires & Laboratoire Jacques-Louis Lions, Université Paris Diderot, 75205 Paris Cedex 13, France (garnier@math.univ-paris-diderot.fr). This author's work was supported in part by ERC Advanced Grant Project MULTIMOD-267184.

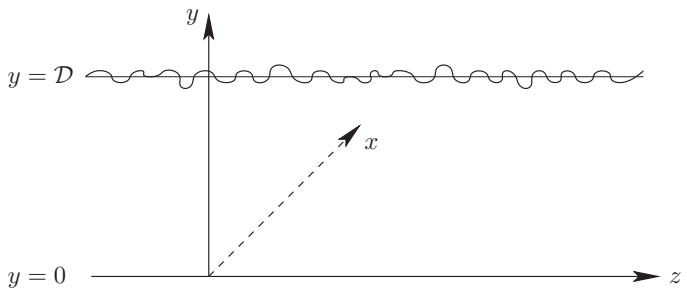

FIG. 1. *Schematic of the problem setup. The system of coordinates has range origin $z = 0$ at the source. The rigid bottom boundary $y = 0$ is assumed flat, and the pressure release top boundary has fluctuations around the value $y = \mathcal{D}$. The cross-range x and the range z are unbounded, that is, $(x, z) \in \mathbb{R}^2$.*

The bottom of the waveguide is assumed rigid,

$$\partial_y p(t, x, y = 0, z) = 0, \tag{1.3}$$

and we take a pressure release boundary condition at the perturbed top boundary,

$$p(t, x, y = T(x, z), z) = 0. \tag{1.4}$$

Perturbed means that the boundary $y = T(x, z)$ has small fluctuations around the mean depth $\mathcal{D}$,

$$|T(x, z) - \mathcal{D}| \ll \mathcal{D}. \tag{1.5}$$

We choose this setup for simplicity. The results extend readily to other boundary conditions and to fluctuating bottoms. Such boundaries were considered recently in [1, 14], in two-dimensional waveguides. Extensions to media with small (x, y, z)-dependent random fluctuations of the wave speed can also be made using the techniques developed in [15, 8, 11, 12, 13].

The goal of our study is to quantify the effect of scattering at the surface. Because in applications it is not feasible to know the boundary fluctuations in detail, we model them with a random process. The solution $p(t, x, y, z)$ of (1.1)–(1.4) is therefore a random field, and we describe in detail its statistics at long ranges, where cumulative scattering is significant. We use the results for two applications: time reversal and sensor array imaging.

Our method of solution uses a change of coordinates to straighten the boundary. The transformed problem has a simple geometry but a randomly perturbed differential operator. Its solution is given by a superposition of propagating and evanescent waveguide modes of the unperturbed waveguide, with random amplitudes. We show that in the long range limit these amplitudes satisfy a system of paraxial equations that are driven by a Brownian field. The detailed characterization of the statistics of $p(t, x, y, z)$ follows from this system. It involves the calculation of the mode-dependent scattering mean free path, which is the distance over which the modes lose coherence; the mode-dependent decoherence length, which is the cross-range offset over which the mode amplitudes decorrelate; and the mode-dependent decoherence frequency, which is the frequency offset over which the mode amplitudes decorrelate. These scales are important in studies of time reversal and imaging, because they dictate

the resolution of focusing and the robustness (statistical stability) of the results with respect to realizations of the random fluctuations of the boundary.

We use the characterization of the statistics of the acoustic pressure field to study the refocusing of the waves in the time reversal process and the resolution of imaging the source with a remote array of sensors. In time reversal the waves received at the array are reversed in time and reemitted in the medium where they propagate back to the original source and refocus. The interesting result is that the refocusing is improved (has superresolution) in random waveguides, especially for long recording times that capture many modes arriving at the array, and it is robust with respect to the realization of the random boundary, as long as the array has a large enough aperture, or the emitted signals have large enough bandwidth. The superresolution property of the time reversal process in random media has received much attention, beginning with the work in [10, 16], and has been analyzed mathematically in detail for wave propagation in open space [2, 3, 20] and in two-dimensional waveguides [12]. Here we analyze it for the three-dimensional random waveguides defined above and describe in detail the improved resolution and robustness of the refocusing.

Imaging is very different from time reversal. While in time reversal the waves propagate physically in the real medium from the array to the source, in imaging they are propagated analytically or computationally. Because the boundary fluctuations are not known, the propagation is done in a fictitious waveguide with planar (unperturbed) boundary. We show that the resulting imaging function is not useful for imaging sources at long distances from the array, beyond the scattering mean free paths of all the waveguide modes. The strong cumulative scattering at the surface causes large random fluctuations of the wave field p (the waveguide noise) that exceed its expectation (the signal). The signal to noise ratio (SNR) is low, and the images are unreliable; they lack statistical stability. Note that the array data corresponds to the pressure measured for a single realization of the random boundary. The image is formed by processing these data, and statistical stability means that the result is essentially independent of the boundary fluctuations, which are unknown.

We show that imaging can be carried out at long ranges by propagating local cross-correlations of the array data. Local means that the cross-correlations are computed for the data projected on one waveguide mode at a time and for nearby cross-ranges and frequencies. The superposition of the local cross-correlations propagated analytically or computationally to the search domain in the fictitious waveguide with unperturbed boundary forms an imaging function that is similar to the coherent interferometric (CINT) one introduced and analyzed in [7, 5, 6, 4] for imaging in open random environments. We analyze in detail the resolution limits of the imaging method and show that it is statistically stable under the same conditions as time reversal: for large enough apertures or bandwidths. However, while cumulative scattering improves the refocusing in time reversal, it impedes imaging. The resolution is worse than in unperturbed waveguides, and it does not improve by increasing the recording time.

The paper is organized as follows: We begin in section 2 with the unperturbed problem, in ideal (unperturbed) waveguides with planar boundaries, and introduce the mode decomposition of the wave field. We consider sources that emit a beam along the range direction and introduce in section 3 the paraxial scaling regime for beam propagation and the random model of the boundary fluctuations. The analysis of beam propagation in random waveguides is in section 4. We may view it as a perturbation of that in ideal waveguides, in the sense that the wave field can be decomposed

in the same waveguide modes. However, the modes are coupled by scattering at the random boundary and have random amplitudes. The random boundary fluctuations are small, but they have a significant cumulative scattering effect at long ranges, as described in section 5. The statistics of the wave field at long ranges are described in section 6. The results are summarized in section 7 and are used in sections 8 and 9 for analyzing time reversal and imaging with sensor arrays. We end with a summary in section 10.

2. The unperturbed problem and mode decomposition. The pressure field in ideal waveguides, with planar boundaries, is given by

$$p_o(t,x,y,z) = \int_{-\infty}^{\infty} \frac{d\omega}{2\pi}\, \widehat{p}_o(\omega,x,y,z)e^{-i\omega t}, \tag{2.1}$$

with Fourier coefficients satisfying a separable problem for the Helmholtz equation

$$\left[\partial_x^2 + \partial_y^2 + \partial_z^2 + \frac{\omega^2}{c^2(y)}\right]\widehat{p}_o(\omega,x,y,z) = \widehat{f}(\omega,x,y)\delta(z), \tag{2.2}$$

$$|\omega-\omega_0| \le \frac{B}{2}, \quad (x,z)\in\mathbb{R}^2, \quad y\in(0,\mathcal{D}),$$

with boundary conditions

$$\partial_y \widehat{p}_o(\omega,x,y=0,z) = \widehat{p}_o(\omega,x,y=\mathcal{D},z) = 0 \tag{2.3}$$

and outgoing radiation conditions at $\sqrt{x^2+z^2}\to\infty$. The Fourier transform of the source

$$\widehat{f}(\omega,x,y) = \int_{-\infty}^{\infty} dt\, f(t,x,y)e^{i\omega t} \tag{2.4}$$

is assumed to be compactly supported in $[\omega_0 - B/2, \omega_0 + B/2]$ for any x and y. Here ω_0 is the central frequency and B is the bandwidth. The spatial (cross-range) support of the source $\widehat{f}(\omega,x,y)$ is larger than the wavelength, as described in detail in section 3, so that it emits a beam in the range direction z.

The boundary value problem (2.2)–(2.3) for the Helmholtz equation can be solved with separation of variables. The solution is a superposition of $N(\omega)$ propagating modes, and infinitely many evanescent ones,

$$\widehat{p}_o(\omega,x,y,z) = \sum_{j=1}^{N(\omega)} \phi_j(\omega,y)\widehat{u}_{j,o}(\omega,x,z) + \sum_{j=N(\omega)+1}^{\infty} \phi_j(\omega,y)\widehat{v}_{j,o}(\omega,x,z). \tag{2.5}$$

The decomposition is in the $L^2(0,\mathcal{D})$ orthonormal basis of the eigenfunctions $\phi_j(\omega,y)$ of the self-adjoint differential operator in y,

$$\left[\partial_y^2 + \frac{\omega^2}{c^2(y)}\right]\phi_j(\omega,y) = \lambda_j(\omega)\phi_j(\omega,y),$$

$$\phi_j(\omega,\mathcal{D}) = \partial_y\phi_j(\omega,0) = 0, \qquad j=1,2,\ldots,$$

with eigenvalues $\lambda_j(\omega)$ that are simple [21].

To simplify the analysis, we assume in this paper that the wave speed is homogeneous:

$$c(y) = c_o. \tag{2.6}$$

The results for variable $c(y)$ are similar in all the essential aspects, as long as the wave speed profile does not trap the eigenfunctions in the interior of the waveguide, away from the surface. The simplification brought by (2.6) amounts to having explicit expressions of the eigenfunctions, which are independent of the frequency

$$\phi_j(y) = \sqrt{\frac{2}{\mathcal{D}}} \cos\left[\pi\left(j - \frac{1}{2}\right)\frac{y}{\mathcal{D}}\right]. \tag{2.7}$$

The eigenvalues are

$$\lambda_j(\omega) = \left(\frac{\pi}{\mathcal{D}}\right)^2 \left[\left(\frac{k\mathcal{D}}{\pi}\right)^2 - \left(j - \frac{1}{2}\right)^2\right], \tag{2.8}$$

where $k = \omega/c_o$ is the wavenumber, and only the first $N(\omega)$ of them are nonnegative:

$$N(\omega) = \left\lfloor \frac{k\mathcal{D}}{\pi} + \frac{1}{2} \right\rfloor. \tag{2.9}$$

The notation $\lfloor\ \rfloor$ stands for the integer part. We suppose for simplicity that $N(\omega)$ remains constant in the bandwidth $[\omega_0 - B/2, \omega_0 + B/2]$ and from now on write $N(\omega) = N$.

The propagating components in (2.5) satisfy the two-dimensional Helmholtz equation

$$\left[\partial_x^2 + \partial_z^2 + \beta_j^2(\omega)\right] \widehat{u}_{j,o}(\omega, x, z) = \widehat{F}_j(\omega, x)\delta(z), \qquad j = 1, \ldots, N, \tag{2.10}$$

with outgoing, radiation conditions at $\sqrt{x^2 + z^2} \to \infty$. The evanescent components solve

$$\left[\partial_x^2 + \partial_z^2 - \beta_j^2(\omega)\right] \widehat{v}_{j,o}(\omega, x, z) = \widehat{F}_j(\omega, x)\delta(z), \qquad j > N, \tag{2.11}$$

with decay condition $\widehat{v}_{j,o}(\omega, x, z) \to 0$ at $\sqrt{x^2 + z^2} \to \infty$. Here we introduce the coefficients of the source profile in the basis of the eigenfunctions

$$\widehat{F}_j(\omega, x) = \int_0^{\mathcal{D}} dy\, \phi_j(y) \widehat{f}(\omega, x, y), \qquad j \geq 1, \tag{2.12}$$

and the mode wavenumbers

$$\beta_j(\omega) = \sqrt{|\lambda_j(\omega)|} = \frac{\pi}{\mathcal{D}} \sqrt{\left|\left(\frac{k\mathcal{D}}{\pi}\right)^2 - \left(j - \frac{1}{2}\right)^2\right|}, \qquad j \geq 1. \tag{2.13}$$

We assume that none of the $\beta_j(\omega)$ vanishes in the bandwidth, so that there are no standing waves. That is to say,

$$\frac{k\mathcal{D}}{\pi} = N + \alpha(\omega) - \frac{1}{2}, \qquad \alpha(\omega) \in (0, 1) \ \text{ for all } \ \omega \in [\omega_0 - B/2, \omega_0 + B/2]. \tag{2.14}$$

3. The paraxial scaling regime and the random model. We define in section 3.1 the paraxial scaling regime and the random model of the boundary fluctuations. The source has a cross-range profile that extends over many wavelengths and emits a beam along the range axis z. The beam propagation in ideal waveguides is described in section 3.2. We use it as a reference to compare with the result in random waveguides derived in section 4.

3.1. Scaling and the random boundary fluctuations. The source is of the form

$$f^\varepsilon(t,x,y) = f(t,\varepsilon x,y), \tag{3.1}$$

where

$$\varepsilon = \frac{\lambda_0}{r_0} \ll 1 \tag{3.2}$$

is a small dimensionless parameter defined as the ratio of the central wavelength λ_0 and the transverse width r_0 of the source. Standard diffraction theory gives that the Rayleigh length for a beam with initial width r_0 is of the order of

$$r_0^2/\lambda_0 = \lambda_0/\varepsilon^2.$$

The Rayleigh length is defined as the distance along the z axis from the beam waist to the place where the beam area is doubled by diffraction. To capture order one diffraction effects we analyze the wave field at $O(\varepsilon^{-1})$ cross-range scales, similar to r_0, and at range scale L^ε, similar to the Rayleigh length

$$L^\varepsilon/\lambda_0 = O(\varepsilon^{-2}). \tag{3.3}$$

The boundary fluctuations are modeled with a random process μ:

$$T^\varepsilon(x,z) = \mathcal{D}\left[1+\varepsilon^{3/2}\mu\left(\varepsilon x,\varepsilon z\right)\right], \qquad z\in(0,L/\varepsilon^2). \tag{3.4}$$

The process μ is bounded, zero-mean, stationary, and mixing, meaning in particular that its covariance is integrable.[1] Because our method of solution flattens the boundary by changing coordinates, we require that μ be twice differentiable, with almost surely bounded derivatives. Its covariance function is given by

$$R\left(\xi,\zeta\right) = \mathbb{E}\left[\mu(\xi'+\xi,\zeta'+\zeta)\mu(\xi',\zeta')\right], \tag{3.5}$$

and we denote by $R_o(\xi)$ its integral over ζ,

$$R_o(\xi) = \int_{-\infty}^{\infty} d\zeta\, R(\xi,\zeta). \tag{3.6}$$

Our assumption on the differentiability of μ implies that R_o is four times differentiable. Note that $\xi=0$ is the maximum of the integrated covariance $R_o(\xi)$, so we have

$$R_o'(0) = 0. \tag{3.7}$$

As seen in (3.4) we assume that the correlation length ℓ^ε of the fluctuations of the boundary is of the same order as the beam width

$$\ell^\varepsilon = \varepsilon^{-1}\ell \sim r_0, \tag{3.8}$$

so that there is nontrivial interaction between the random boundary and the wave beam. The amplitude of the fluctuations is scaled to order of $\varepsilon^{3/2}\lambda_0$, in order to obtain a cumulative scattering effect of order one after the propagation distance L^ε.

[1] More precisely, μ is a $\mathfrak{f}$-mixing process, with $\mathfrak{f}\in L^{1/2}(\mathbb{R}^+)$, as stated in [17, sect. 4.6.2].

Weaker fluctuations have a negligible effect, and stronger fluctuations cause so much scattering that coherent imaging at range scale L^ε is no longer possible. In (3.8) we denote by ℓ the scaled (order one) correlation length defined by

$$R_o(0) = \sigma^2 \ell, \qquad \frac{R_o''(0)}{R_o(0)} = -\frac{1}{\ell^2}, \tag{3.9}$$

and σ is the typical amplitude of μ.

We use the hyperbolicity of the problem to truncate mathematically the boundary fluctuations to the range interval $(0, L/\varepsilon^2)$. The upper bound L/ε^2 is the maximum range of the fluctuations that can affect the waves up to an observation time scaled as $O\big(L/(\varepsilon^2 c_o)\big)$. The lower bound 0 in the range interval coincides with the location of the source. It is motivated by two facts: First, we observe the waves at positive ranges. Second, the backscattered field is negligible in the scaling regime defined above, as we show later in section 5.3.

3.2. Beam propagation in ideal waveguides. We rename the field in the paraxial scaling defined above as

$$p_o^\varepsilon(t, X, y, Z) = p_o\left(t, \frac{X}{\varepsilon}, y, \frac{Z}{\varepsilon^2}\right). \tag{3.10}$$

Its Fourier coefficients are given by the scaled version of (2.5),

$$\widehat{p}_o^{\,\varepsilon}(\omega, X, y, Z) = \sum_{j=1}^{N(\omega)} \phi_j(y) \widehat{u}_{j,o}^{\,\varepsilon}(\omega, X, Z) + \sum_{j=N(\omega)+1}^{\infty} \phi_j(y) \widehat{v}_{j,o}^{\,\varepsilon}(\omega, X, Z), \tag{3.11}$$

with propagating mode amplitudes $\widehat{u}_{j,o}^{\,\varepsilon}$ satisfying the scaled equation (2.10), with the source replaced by $\widehat{F}_j(\omega, \varepsilon x = X)$. They can be written as

$$\widehat{u}_{j,o}^{\,\varepsilon}(\omega, X, Z) = -\frac{1}{\varepsilon} \int_{-\infty}^{\infty} dX'\, \widehat{F}_j(\omega, X') \widehat{G}_o\left(\beta_j(\omega), \frac{X - X'}{\varepsilon}, \frac{Z}{\varepsilon^2}\right)$$

in terms of the outgoing Green's function

$$\widehat{G}_o\big(\beta_j(\omega), x, z\big) = \frac{i}{4} H_0^{(1)}\left[\beta_j(\omega)\sqrt{x^2 + z^2}\right].$$

Here $H_0^{(1)}$ is the Hankel function of the first kind, and because $\varepsilon \ll 1$, we can use its asymptotic form for a scaled range $Z > 0$:

$$\begin{aligned}
\frac{i}{4} H_0^{(1)}\left[\beta_j(\omega)\sqrt{\frac{(X-X')^2}{\varepsilon^2} + \frac{Z^2}{\varepsilon^4}}\right] &\approx \frac{1}{4}\left[\frac{2i}{\pi\beta_j(\omega)\sqrt{\frac{(X-X')^2}{\varepsilon^2} + \frac{Z^2}{\varepsilon^4}}}\right]^{1/2} \\
&\quad \times \exp\left[i\beta_j(\omega)\sqrt{\frac{(X-X')^2}{\varepsilon^2} + \frac{Z^2}{\varepsilon^4}}\right] \\
&\approx \frac{\varepsilon}{2}\sqrt{\frac{i}{2\pi\beta_j(\omega)Z}} \exp\left\{i\beta_j(\omega)\left[\frac{Z}{\varepsilon^2} + \frac{(X-X')^2}{2Z}\right]\right\}.
\end{aligned}$$

The propagating components of the wave field become

$$\widehat{u}_{j,o}^{\,\varepsilon}(\omega, X, Z) \approx a_{j,o}(\omega, X, Z) \exp\left[i\beta_j(\omega)\frac{Z}{\varepsilon^2}\right],$$

with

$$a_{j,o}(\omega,X,Z)=-\frac{1}{2}\sqrt{\frac{i}{2\pi\beta_j(\omega)Z}}\int_{-\infty}^{\infty}dX'\,\exp\left[\frac{i\beta_j(\omega)(X-X')^2}{2Z}\right]\widehat{F}_j(\omega,X') \tag{3.12}$$

for $j=1,\ldots,N$. The evanescent components are obtained similarly from (2.11):

$$\widehat{v}^{\varepsilon}_{j,o}(\omega,X,Z)\approx e_{j,o}(\omega,X,Z)\exp\left[-\beta_j(\omega)\frac{Z}{\varepsilon^2}\right],$$

and

$$e_{j,o}(\omega,X,Z)=-\frac{1}{2}\sqrt{\frac{1}{2\pi\beta_j(\omega)Z}}\int_{-\infty}^{\infty}dX'\,\exp\left[-\frac{\beta_j(\omega)(X-X')^2}{2Z}\right]\widehat{F}_j(\omega,X') \tag{3.13}$$

for $j\geq N+1$. These modes are exponentially damped and can be neglected.

In summary, the paraxial approximation of the wave field is given by

$$\widehat{p}^{\varepsilon}_o(\omega,X,y,Z)\approx\sum_{j=1}^{N}\phi_j(y)a_{j,o}(\omega,X,Z)e^{i\beta_j(\omega)\frac{Z}{\varepsilon^2}}. \tag{3.14}$$

It is a superposition of forward-going modes, which are quasi-plane waves propagating in the range direction z, with slowly varying amplitudes $a_{j,o}$ given by (3.12). They solve the paraxial equations

$$\left[2i\beta_j(\omega)\partial_Z+\partial_X^2\right]a_{j,o}(\omega,X,Z)=0,\qquad j=1,\ldots,N, \tag{3.15}$$

with initial conditions

$$a_{j,o}(\omega,X,Z=0)=a_{j,\mathrm{ini}}(\omega,X):=\frac{1}{2i\beta_j(\omega)}\widehat{F}_j(\omega,X),\qquad j=1,\ldots,N. \tag{3.16}$$

4. Wave propagation in random waveguides. To analyze beam propagation in random waveguides we introduce in section 4.1 a change of coordinates that flattens the random boundary. The mapped wave field satisfies a wave equation perturbed by a differential operator with random coefficients defined by the process μ. We show in section 4.2 that the solution can be written as a superposition of the unperturbed waveguide modes with random amplitudes that solve paraxial equations driven by the random process μ. They model the cumulative scattering effects of the random boundary and are analyzed in section 5 in the paraxial scaling regime defined in section 3.

4.1. Change of coordinates. Consider the change of coordinates from (x,y,z) to (x,η,z), with

$$\eta=\frac{y\mathcal{D}}{T^{\varepsilon}(x,z)}, \tag{4.1}$$

which straightens the boundary $y=T^{\varepsilon}(x,z)$ to $\eta=\mathcal{D}$ for any $x\in\mathbb{R}$ and $z\in(0,L/\varepsilon^2)$. The pressure field in the new coordinates is denoted by

$$\widehat{P}(\omega,x,\eta,z)=\widehat{p}\left(\omega,x,\frac{\eta T^{\varepsilon}(x,z)}{\mathcal{D}},z\right). \tag{4.2}$$

It satisfies the simple boundary conditions

$$\widehat{P}(\omega, x, \mathcal{D}, z) = \partial_\eta \widehat{P}(\omega, x, 0, z) = 0 \tag{4.3}$$

and the partial differential equation

$$\begin{aligned}\Big[\partial_x^2 + \partial_z^2 + \Big(\frac{\mathcal{D}^2}{{T^\varepsilon}^2} + \eta^2 \frac{|\nabla T^\varepsilon|^2}{{T^\varepsilon}^2}\Big)\partial_\eta^2 - 2\eta \frac{\nabla T^\varepsilon}{T^\varepsilon}\cdot\nabla\partial_\eta \\ + \Big(2\eta \frac{|\nabla T^\varepsilon|^2}{{T^\varepsilon}^2} - \eta \frac{\Delta T^\varepsilon}{T^\varepsilon}\Big)\partial_\eta + k^2\Big]\widehat{P} = \widehat{f}^\varepsilon(\omega, x, \eta)\delta(z),\end{aligned} \tag{4.4}$$

derived from (1.1) and (4.2) using the chain rule. Here ∇ and Δ are the gradient and Laplacian operators in (x, z) and f^ε is the source of the form (3.1).

When substituting the model (3.4) into (4.4), we obtain that $\widehat{P}$ satisfies a randomly perturbed problem

$$\Big[\partial_x^2 + \partial_z^2 + \Big(1 - 2\varepsilon^{3/2}\mu(\varepsilon x, \varepsilon z)\Big)\partial_\eta^2 + k^2 + h.o.t.\Big]\widehat{P}(\omega, x, \eta, z) = \widehat{f}(\omega, \varepsilon x, \eta)\delta(z). \tag{4.5}$$

The higher-order terms *h.o.t.* are

$$h.o.t. = r_1^\varepsilon(\varepsilon x, \eta, \varepsilon z)\partial_\eta^2 + r_2^\varepsilon(\varepsilon x, \eta, \varepsilon z)\partial_{\eta x}^2 + r_3^\varepsilon(\varepsilon x, \eta, \varepsilon z)\partial_{\eta z}^2 + r_4^\varepsilon(\varepsilon x, \eta, \varepsilon z)\partial_\eta,$$

with functions

$$\begin{aligned} r_1^\varepsilon &= \frac{\varepsilon^3\mu^2(3 + 2\varepsilon^{3/2}\mu)}{(1 + \varepsilon^{3/2}\mu)^2} + \varepsilon^5\eta^2\frac{(\partial_\xi\mu)^2 + (\partial_\zeta\mu)^2}{(1 + \varepsilon^{3/2}\mu)^2}, \\ r_2^\varepsilon &= -2\varepsilon^{5/2}\eta\frac{\partial_\xi\mu}{1 + \varepsilon^{3/2}\mu}, \\ r_3^\varepsilon &= -2\varepsilon^{5/2}\eta\frac{\partial_\zeta\mu}{1 + \varepsilon^{3/2}\mu}, \\ r_4^\varepsilon &= 2\varepsilon^5\eta\frac{(\partial_\xi\mu)^2 + (\partial_\zeta\mu)^2}{(1 + \varepsilon^{3/2}\mu)^2} - \varepsilon^{7/2}\eta\frac{\partial_\xi^2\mu + \partial_\zeta^2\mu}{1 + \varepsilon^{3/2}\mu}, \end{aligned}$$

evaluated at arguments $(\varepsilon x, \eta, \varepsilon z)$. These terms are called higher-order because they turn out to be negligible in the limit $\varepsilon \to 0$ considered in section 5.

4.2. Wave decomposition. Equation (4.5) is not separable, but we can still write its solution in the $L^2(0, \mathcal{D})$ basis of the eigenfunctions (2.7). The expansion is similar to (2.5):

$$\widehat{P}(\omega, x, \eta, z) = \sum_{j=1}^{N} \phi_j(\eta)\widehat{u}_j(\omega, x, z) + \sum_{j>N} \phi_j(\eta)\widehat{v}_j(\omega, x, z). \tag{4.6}$$

We define the forward- and backward-going wave mode amplitudes a_j and b_j by

$$\begin{aligned} a_j(\omega, x, z) &= \Big(\frac{1}{2}\widehat{u}_j(\omega, x, z) + \frac{1}{2i\beta_j(\omega)}\partial_z\widehat{u}_j(\omega, x, z)\Big)e^{-i\beta_j(\omega)z}, \\ b_j(\omega, x, z) &= \Big(\frac{1}{2}\widehat{u}_j(\omega, x, z) - \frac{1}{2i\beta_j(\omega)}\partial_z\widehat{u}_j(\omega, x, z)\Big)e^{i\beta_j(\omega)z}, \end{aligned} \tag{4.7}$$

so that the complex valued amplitudes of the propagating modes can be written as

$$\widehat{u}_j(\omega,x,z) = a_j(\omega,x,z)e^{i\beta_j(\omega)z} + b_j(\omega,x,z)e^{-i\beta_j(\omega)z}. \tag{4.8}$$

Definition (4.7) implies that the complex mode amplitudes also satisfy

$$\partial_z a_j(\omega,x,z)e^{i\beta_j(\omega)z} + \partial_z b_j(\omega,x,z)e^{-i\beta_j(\omega)z} = 0. \tag{4.9}$$

Equations (4.8) and (4.9) uniquely specify the propagating mode amplitudes. They each satisfy a single boundary condition in the range $(0, L/\varepsilon^2)$ of the fluctuations. To derive these boundary conditions, let us observe that because the boundary is flat outside $(0, L/\varepsilon^2)$, the radiation (outgoing conditions) implies that the mode amplitudes satisfy

$$a_j(\omega,x,z=0^-) = 0, \tag{4.10}$$

$$b_j(\omega,x,z=L/\varepsilon^2) = 0. \tag{4.11}$$

The last equation is the boundary condition for b_j. The boundary value $a_j(\omega,x,z=0^+)$ follows from the jump conditions across the plane $z=0$ of the source in (4.5). We have

$$[\widehat{u}_j]_{0^-}^{0^+} = 0, \quad [\partial_z \widehat{u}_j]_{0^-}^{0^+} = \widehat{F}_j(\omega,\varepsilon x),$$

with $\widehat{F}_j$ defined by (2.12). This gives

$$[a_j + b_j]_{0^-}^{0^+} = 0, \quad i\beta_j[a_j - b_j]_{0^-}^{0^+} = \widehat{F}_j(\omega,\varepsilon x),$$

and therefore

$$a_j(\omega,x,0^+) = \frac{1}{2i\beta_j(\omega)}\widehat{F}_j(\omega,\varepsilon x). \tag{4.12}$$

Substituting (4.6) into (4.5) and using the orthonormality of the eigenfunctions ϕ_j, we find that the wave mode amplitudes solve paraxial equations coupled by the random fluctuations in $z \in (0, L/\varepsilon^2)$,

$$\begin{aligned}
&\big(2i\beta_j\partial_z + \partial_x^2\big)a_j + e^{-2i\beta_j z}\partial_x^2 b_j \\
&= \varepsilon^{3/2}\mu(\varepsilon x,\varepsilon z)e^{-i\beta_j z}\left[\sum_{l=1}^{N} q_{jl}\big(a_l e^{i\beta_l z} + b_l e^{-i\beta_l z}\big) + \sum_{l>N} q_{jl}\widehat{v}_l\right] \\
&\quad + \mathcal{E}_{j,\mathbf{a}}(\mathbf{a},\mathbf{b},\varepsilon x,\varepsilon z)
\end{aligned} \tag{4.13}$$

and

$$\begin{aligned}
&\big(-2i\beta_j\partial_z + \partial_x^2\big)b_j + e^{2i\beta_j z}\partial_x^2 a_j \\
&= \varepsilon^{3/2}\mu(\varepsilon x,\varepsilon z)e^{i\beta_j z}\left[\sum_{l=1}^{N} q_{jl}\big(a_l e^{i\beta_l z} + b_l e^{-i\beta_l z}\big) + \sum_{l>N} q_{jl}\widehat{v}_l\right] \\
&\quad + \mathcal{E}_{j,\mathbf{b}}(\mathbf{a},\mathbf{b},\varepsilon x,\varepsilon z),
\end{aligned} \tag{4.14}$$

with remainders defined by

$$\begin{aligned}\mathcal{E}_{j,\mathbf{a}}(\mathbf{a},\mathbf{b},\varepsilon x,\varepsilon z) = &-\sum_{l=1}^{N} e^{i(\beta_l-\beta_j)z}\big[r_{jl}^{1,\varepsilon}(\varepsilon x,\varepsilon z)a_l + i\beta_l r_{jl}^{3,\varepsilon}(\varepsilon x,\varepsilon z)a_l \\ &\qquad + r_{jl}^{2,\varepsilon}(\varepsilon x,\varepsilon z)\partial_x a_l + r_{jl}^{3,\varepsilon}(\varepsilon x,\varepsilon z)\partial_z a_l\big] \\ &-\sum_{l=1}^{N} e^{i(-\beta_l-\beta_j)z}\big[r_{jl}^{1,\varepsilon}(\varepsilon x,\varepsilon z)b_l - i\beta_l r_{jl}^{3,\varepsilon}(\varepsilon x,\varepsilon z)b_l \\ &\qquad + r_{jl}^{2,\varepsilon}(\varepsilon x,\varepsilon z)\partial_x b_l + r_{jl}^{3,\varepsilon}(\varepsilon x,\varepsilon z)\partial_z b_l\big] \\ &-\sum_{l>N} e^{-i\beta_j z}\big[r_{jl}^{1,\varepsilon}(\varepsilon x,\varepsilon z)\widehat{v}_l + r_{jl}^{2,\varepsilon}(\varepsilon x,\varepsilon z)\partial_x\widehat{v}_l + r_{jl}^{3,\varepsilon}(\varepsilon x,\varepsilon z)\partial_z\widehat{v}_l\big]\end{aligned}$$

and

$$\begin{aligned}\mathcal{E}_{j,\mathbf{b}}(\mathbf{a},\mathbf{b},\varepsilon x,\varepsilon z) = &-\sum_{l=1}^{N} e^{i(\beta_l+\beta_j)z}\big[r_{jl}^{1,\varepsilon}(\varepsilon x,\varepsilon z)a_l + i\beta_l r_{jl}^{3,\varepsilon}(\varepsilon x,\varepsilon z)a_l \\ &\qquad + r_{jl}^{2,\varepsilon}(\varepsilon x,\varepsilon z)\partial_x a_l + r_{jl}^{3,\varepsilon}(\varepsilon x,\varepsilon z)\partial_z a_l\big] \\ &-\sum_{l=1}^{N} e^{i(-\beta_l+\beta_j)z}\big[r_{jl}^{1,\varepsilon}(\varepsilon x,\varepsilon z)b_l - i\beta_l r_{jl}^{3,\varepsilon}(\varepsilon x,\varepsilon z)b_l \\ &\qquad + r_{jl}^{2,\varepsilon}(\varepsilon x,\varepsilon z)\partial_x b_l + r_{jl}^{3,\varepsilon}(\varepsilon x,\varepsilon z)\partial_z b_l\big] \\ &-\sum_{l>N} e^{i\beta_j z}\big[r_{jl}^{1,\varepsilon}(\varepsilon x,\varepsilon z)\widehat{v}_l + r_{jl}^{2,\varepsilon}(\varepsilon x,\varepsilon z)\partial_x\widehat{v}_l + r_{jl}^{3,\varepsilon}(\varepsilon x,\varepsilon z)\partial_z\widehat{v}_l\big]\end{aligned}$$

in terms of

$$\begin{aligned} r_{jl}^{1,\varepsilon}(\varepsilon x,\varepsilon z) &= \int_0^{\mathcal{D}} d\eta\big[\phi_j(\eta)\phi_l''(\eta)r_1^{\varepsilon}(\varepsilon x,\eta,\varepsilon z) + \phi_j(\eta)\phi_l'(\eta)r_4^{\varepsilon}(\varepsilon x,\eta,\varepsilon z)\big], \\ r_{jl}^{2,\varepsilon}(\varepsilon x,\varepsilon z) &= \int_0^{\mathcal{D}} d\eta\,\phi_j(\eta)\phi_l'(\eta)r_2^{\varepsilon}(\varepsilon x,\eta,\varepsilon z), \\ r_{jl}^{3,\varepsilon}(\varepsilon x,\varepsilon z) &= \int_0^{\mathcal{D}} d\eta\,\phi_j(\eta)\phi_l'(\eta)r_3^{\varepsilon}(\varepsilon x,\eta,\varepsilon z).\end{aligned}$$

Note that $r_{jl}^{q,\varepsilon} = O(\varepsilon^{5/2})$ for $q = 1, 2, 3$.

The leading coupling matrix in (4.13)–(4.14) is given by

$$q_{jl} = 2\int_0^{\mathcal{D}} d\eta\,\phi_j(\eta)\phi_l''(\eta) = -2\left(\frac{\pi}{\mathcal{D}}\right)^2\left(j-\frac{1}{2}\right)^2\delta_{jl}. \tag{4.15}$$

It takes this simple diagonal form, because we assumed a homogeneous background speed c_o. If we had a variable speed $c(y)$, the matrix $\{q_{jl}\}$ would not be diagonal, and the modes with $j \neq l$ would be coupled. However, the results of the asymptotic analysis below would still hold, because the coupling would become negligible in the limit $\varepsilon \to 0$ considered in section 5, due to rapid phase terms $\exp(i(\pm\beta_j \pm \beta_l)z)$ arising in the right-hand sides of (4.13), (4.14).

The equations for the evanescent components are obtained similarly,

$$\big(\partial_z^2 + \partial_x^2 - \beta_j^2\big)\,\widehat{v}_j \approx \varepsilon^{3/2}\mu(\varepsilon x,\varepsilon z)\,q_{jj}\widehat{v}_j, \tag{4.16}$$

with higher-order terms as in (4.13)–(4.14), and they are augmented with the decay conditions $\widehat{v}_j(\omega, x, z) \to 0$ as $\sqrt{x^2+z^2} \to \infty$ for all $j \geq N+1$. The equations for the evanescent mode amplitudes are similar to those encountered in [1]. These amplitudes were shown to vanish as $\varepsilon \to 0$ in [1, sect. 3.3] in a regime that was similar to that addressed in this paper. We therefore neglect them in the following.

5. The limit process. We characterize next the wave field in the asymptotic limit $\varepsilon \to 0$. We begin with the paraxial long range scaling that gives significant net scattering and then take the limit. The scaling has already been described in section 3.1.

5.1. Asymptotic scaling. We obtain from (4.13)–(4.15) that the propagating mode amplitudes satisfy the system of partial differential equations

$$\begin{aligned}
&\begin{pmatrix} 2i\beta_j\partial_z + \partial_x^2 & e^{-2i\beta_j z}\partial_x^2 \\ e^{2i\beta_j z}\partial_x^2 & -2i\beta_j\partial_z + \partial_x^2 \end{pmatrix} \begin{pmatrix} a_j \\ b_j \end{pmatrix} = \varepsilon^{3/2} q_{jj}\mu(\varepsilon x, \varepsilon z) \begin{pmatrix} 1 & e^{-2i\beta_j z} \\ e^{2i\beta_j z} & 1 \end{pmatrix} \begin{pmatrix} a_j \\ b_j \end{pmatrix} \\
&\quad - \sum_{l=1}^{N} \begin{pmatrix} e^{-i(\beta_j-\beta_l)z} & e^{-i(\beta_j+\beta_l)z} \\ e^{i(\beta_j+\beta_l)z} & e^{i(\beta_j-\beta_l)z} \end{pmatrix} \big[r_{jl}^{1,\varepsilon}(\varepsilon x, \varepsilon z) + r_{jl}^{2,\varepsilon}(\varepsilon x, \varepsilon z)\partial_x \\
&\qquad\qquad + r_{jl}^{3,\varepsilon}(\varepsilon x, \varepsilon z)\partial_z \big] \begin{pmatrix} a_l \\ b_l \end{pmatrix} \\
&\quad - \sum_{l=1}^{N} \beta_l r_{jl}^{3,\varepsilon}(\varepsilon x, \varepsilon z) \begin{pmatrix} ie^{-i(\beta_j-\beta_l)z} & -ie^{-i(\beta_j+\beta_l)z} \\ ie^{i(\beta_j+\beta_l)z} & -ie^{i(\beta_j-\beta_l)z} \end{pmatrix} \begin{pmatrix} a_l \\ b_l \end{pmatrix}
\end{aligned} \tag{5.1}$$

for $j = 1, \ldots, N$.

Because the leading-order term of the right-hand side in (5.1) is small, of order $\varepsilon^{3/2}$, and has zero statistical expectation, it follows from [11, Chap. 6] that there is no net scattering effect until we reach ranges of order ε^{-2}. Thus, we let

$$z = Z/\varepsilon^2, \tag{5.2}$$

with scaled range Z independent of ε. The source directivity in the range direction suggests observing the wave field on a cross-range scale that is smaller than that in range. We choose it as

$$x = X/\varepsilon, \tag{5.3}$$

with scaled cross-range X independent of ε, to balance the two terms in the paraxial operators in (5.1).

Our goal is to characterize the $\varepsilon \to 0$ limit of the mode amplitudes in the paraxial long range scaling regime (5.2)–(5.3). We denote them by

$$a_j^\varepsilon(\omega, X, Z) = a_j\left(\omega, \frac{X}{\varepsilon}, \frac{Z}{\varepsilon^2}\right) \quad \text{and} \quad b_j^\varepsilon(\omega, X, Z) = b_j\left(\omega, \frac{X}{\varepsilon}, \frac{Z}{\varepsilon^2}\right) \tag{5.4}$$

and obtain from (5.1)–(5.3) that they satisfy the scaled system

$$
\begin{aligned}
&\begin{pmatrix} 2i\beta_j\partial_Z+\partial_X^2 & e^{-2i\beta_j Z/\varepsilon^2}\partial_X^2 \\ e^{2i\beta_j Z/\varepsilon^2}\partial_X^2 & -2i\beta_j\partial_Z+\partial_X^2 \end{pmatrix}\begin{pmatrix} a_j^\varepsilon \\ b_j^\varepsilon \end{pmatrix} \\
&= \frac{1}{\varepsilon^{1/2}}\mu\Big(X,\frac{Z}{\varepsilon}\Big) q_{jj}\begin{pmatrix} 1 & e^{-2i\beta_j Z/\varepsilon^2} \\ e^{2i\beta_j Z/\varepsilon^2} & 1 \end{pmatrix}\begin{pmatrix} a_j^\varepsilon \\ b_j^\varepsilon \end{pmatrix} \\
&\quad -\sum_{l=1}^N \begin{pmatrix} e^{-i(\beta_j-\beta_l)Z/\varepsilon^2} & e^{-i(\beta_j+\beta_l)Z/\varepsilon^2} \\ e^{i(\beta_j+\beta_l)Z/\varepsilon^2} & e^{i(\beta_j-\beta_l)Z/\varepsilon^2} \end{pmatrix} \\
&\quad \times\Big[\frac{1}{\varepsilon^2}r_{jl}^{1,\varepsilon}\Big(X,\frac{Z}{\varepsilon}\Big)+\frac{1}{\varepsilon}r_{jl}^{2,\varepsilon}\Big(X,\frac{Z}{\varepsilon}\Big)\partial_X + r_{jl}^{3,\varepsilon}\Big(X,\frac{Z}{\varepsilon}\Big)\partial_Z\Big]\begin{pmatrix} a_l^\varepsilon \\ b_l^\varepsilon \end{pmatrix} \\
&\quad -\sum_{l=1}^N \frac{1}{\varepsilon^2}\beta_l r_{jl}^{3,\varepsilon}\Big(X,\frac{Z}{\varepsilon}\Big)\begin{pmatrix} ie^{-i(\beta_j-\beta_l)Z/\varepsilon^2} & -ie^{-i(\beta_j+\beta_l)Z/\varepsilon^2} \\ ie^{i(\beta_j+\beta_l)Z/\varepsilon^2} & -ie^{i(\beta_j-\beta_l)Z/\varepsilon^2} \end{pmatrix}\begin{pmatrix} a_l^\varepsilon \\ b_l^\varepsilon \end{pmatrix}
\end{aligned}
\tag{5.5}
$$

for $j=1,\dots,N$, with initial conditions

$$
a_j^\varepsilon(\omega,X,0) = a_{j,\mathrm{ini}}(\omega,X) := \frac{1}{2i\beta_j(\omega)}\widehat{F}_j(\omega,X) \tag{5.6}
$$

and end conditions

$$
b_j^\varepsilon(\omega,X,L) = 0. \tag{5.7}
$$

Note that the higher-order terms in (5.5) (i.e., the terms with $r_{jl}^{q,\varepsilon}$, $q=1,2,3$) are at most of order $O(\varepsilon^{1/2})$.

5.2. The random propagator. Let us rewrite (5.5) in terms of the random propagator matrix $\mathbf{P}^\varepsilon(\omega,X,X',Z)\in\mathbb{C}^{2N\times 2N}$, the solution of the initial value problem

$$
\begin{aligned}
\partial_Z\mathbf{P}^\varepsilon(\omega,X,X',Z) &= \big[\mathbf{I}-\mathbf{L}^\varepsilon(\omega,X,Z)\big]^{-1} \\
&\quad\times\Big[\frac{1}{\varepsilon^{1/2}}\mu\Big(X,\frac{Z}{\varepsilon}\Big)\mathbf{H}\Big(\omega,X,\frac{Z}{\varepsilon^2}\Big)+\mathbf{G}\Big(\omega,X,\frac{Z}{\varepsilon^2}\Big) \\
&\qquad +\mathbf{K}^\varepsilon(\omega,X,Z)\Big]\mathbf{P}^\varepsilon(\omega,X,X',Z), \\
\mathbf{P}^\varepsilon(\omega,X,X',0) &= \delta(X-X')\mathbf{I}.
\end{aligned}
\tag{5.8}
$$

Here $\mathbf{I}$ is the $2N\times 2N$ identity matrix, $\delta(X)$ is the Dirac delta distribution in X, and $\mathbf{G}$ and $\mathbf{H}$ are $2N\times 2N$ matrices with entries given by partial differential operators in X with deterministic coefficients. $\mathbf{K}^\varepsilon$ is a $2N\times 2N$ matrix with entries given by partial differential operators in X, with random coefficients. $\mathbf{L}^\varepsilon$ is a $2N\times 2N$ matrix whose entries are random bounded coefficients. The norm of the matrix is smaller than one for ε small enough, so that the matrix $\mathbf{I}-\mathbf{L}^\varepsilon$ is indeed invertible. We can define these matrices from (5.5) once we note that the solution

$$
\boldsymbol{a}^\varepsilon(\omega,X,Z) = \begin{pmatrix} a_1^\varepsilon(\omega,X,Z) \\ \vdots \\ a_N^\varepsilon(\omega,X,Z)\end{pmatrix}, \qquad \boldsymbol{b}^\varepsilon(\omega,X,Z) = \begin{pmatrix} b_1^\varepsilon(\omega,X,Z) \\ \vdots \\ b_N^\varepsilon(\omega,X,Z)\end{pmatrix} \tag{5.9}
$$

follows from

$$\begin{pmatrix} \boldsymbol{a}^\varepsilon(\omega, X, Z) \\ \boldsymbol{b}^\varepsilon(\omega, X, Z) \end{pmatrix} = \int dX' \, \mathbf{P}^\varepsilon(\omega, X, X', Z) \begin{pmatrix} \boldsymbol{a}^\varepsilon(\omega, X', 0) \\ \boldsymbol{b}^\varepsilon(\omega, X', 0) \end{pmatrix}. \tag{5.10}$$

Here $\boldsymbol{b}^\varepsilon(\omega, X', 0)$ is the vector of backward going amplitudes at the beginning of the randomly perturbed section of the waveguide, and it can be eliminated using the boundary identity

$$\begin{pmatrix} \boldsymbol{a}^\varepsilon(\omega, X, L) \\ \mathbf{0} \end{pmatrix} = \int dX' \, \mathbf{P}^\varepsilon(\omega, X, X', L) \begin{pmatrix} \boldsymbol{a}^\varepsilon(\omega, X', 0) \\ \boldsymbol{b}^\varepsilon(\omega, X', 0) \end{pmatrix}. \tag{5.11}$$

The initial conditions $\boldsymbol{a}^\varepsilon(\omega, X', 0)$ are given in (5.6).

We obtain from (5.5) that $\mathbf{H}$, $\mathbf{G}$, $\mathbf{K}^\varepsilon$, and $\mathbf{L}^\varepsilon$ have the block form

$$\mathbf{H} = \begin{pmatrix} \mathbf{H}^a & \mathbf{H}^b \\ \overline{\mathbf{H}^b} & \overline{\mathbf{H}^a} \end{pmatrix}, \qquad \mathbf{G} = \begin{pmatrix} \mathbf{G}^a & \mathbf{G}^b \\ \overline{\mathbf{G}^b} & \overline{\mathbf{G}^a} \end{pmatrix},$$

$$\mathbf{K}^\varepsilon = \begin{pmatrix} \mathbf{K}^{\varepsilon,a} & \mathbf{K}^{\varepsilon,b} \\ \overline{\mathbf{K}^{\varepsilon,b}} & \overline{\mathbf{K}^{\varepsilon,a}} \end{pmatrix}, \qquad \mathbf{L}^\varepsilon = \begin{pmatrix} \mathbf{L}^{\varepsilon,a} & \mathbf{L}^{\varepsilon,b} \\ \overline{\mathbf{L}^{\varepsilon,b}} & \overline{\mathbf{L}^{\varepsilon,a}} \end{pmatrix}, \tag{5.12}$$

where the bar denotes complex conjugation. The blocks $\mathbf{H}^a$, $\mathbf{H}^b$, $\mathbf{G}^a$, and $\mathbf{G}^b$ are diagonal, with entries

$$\mathbf{H}^a_{jl} = -\frac{i\,\delta_{jl}\,q_{jj}}{2\beta_j}, \qquad \mathbf{H}^b_{jl} = -\frac{i\,\delta_{jl}\,q_{jj}}{2\beta_j} e^{-2i\beta_j Z/\varepsilon^2} \tag{5.13}$$

and

$$\mathbf{G}^a_{jl} = \frac{i\,\delta_{jl}}{2\beta_j}\partial_X^2, \qquad \mathbf{G}^b_{jl} = \frac{i\,\delta_{jl}}{2\beta_j} e^{-2i\beta_j Z/\varepsilon^2}\partial_X^2 \tag{5.14}$$

for $j, l = 1, \ldots, N$. The entries of the diagonal blocks $\mathbf{H}^a$ and $\mathbf{G}^a$ depend only on the mode indices and the frequency, via $\beta_j(\omega)$. The entries of the off-diagonal blocks $\mathbf{H}^b$ and $\mathbf{G}^b$ are rapidly oscillating, due to the large phases proportional to Z/ε^2. The elements of the matrices $\mathbf{K}^{\varepsilon,a}$ and $\mathbf{K}^{\varepsilon,b}$ given by

$$\mathbf{K}^{\varepsilon,a}_{jl} = \frac{i}{2\beta_j} e^{-i(\beta_j-\beta_l)Z/\varepsilon^2} \left[\frac{1}{\varepsilon^2} r^{1,\varepsilon}_{jl}\left(X, \frac{Z}{\varepsilon}\right) + \frac{1}{\varepsilon} r^{2,\varepsilon}_{jl}\left(X, \frac{Z}{\varepsilon}\right)\partial_X + \frac{i}{\varepsilon^2}\beta_l r^{3,\varepsilon}_{jl}\left(X, \frac{Z}{\varepsilon}\right)\right], \tag{5.15}$$

$$\mathbf{K}^{\varepsilon,b}_{jl} = \frac{i}{2\beta_j} e^{-i(\beta_j+\beta_l)Z/\varepsilon^2} \left[\frac{1}{\varepsilon^2} r^{1,\varepsilon}_{jl}\left(X, \frac{Z}{\varepsilon}\right) + \frac{1}{\varepsilon} r^{2,\varepsilon}_{jl}\left(X, \frac{Z}{\varepsilon}\right)\partial_X - \frac{i}{\varepsilon^2}\beta_l r^{3,\varepsilon}_{jl}\left(X, \frac{Z}{\varepsilon}\right)\right] \tag{5.16}$$

are of order $\varepsilon^{1/2}$. The elements of the matrices $\mathbf{L}^{\varepsilon,a}$ and $\mathbf{L}^{\varepsilon,b}$ given by

$$\mathbf{L}^{\varepsilon,a}_{jl} = \frac{i}{2\beta_j} e^{-i(\beta_j-\beta_l)Z/\varepsilon^2} r^{3,\varepsilon}_{jl}\left(X, \frac{Z}{\varepsilon}\right), \qquad \mathbf{L}^{\varepsilon,b}_{jl} = \frac{i}{2\beta_j} e^{-i(\beta_j+\beta_l)Z/\varepsilon^2} r^{3,\varepsilon}_{jl}\left(X, \frac{Z}{\varepsilon}\right) \tag{5.17}$$

are of order $\varepsilon^{5/2}$.

The symmetry relations satisfied by the blocks in $\mathbf{H}$, $\mathbf{G}$, $\mathbf{K}^\varepsilon$, and $\mathbf{L}^\varepsilon$ imply that the propagator has the form

$$\mathbf{P}^\varepsilon(\omega, X, X', Z) = \begin{pmatrix} \mathbf{T}^\varepsilon(\omega, X, X', Z) & \overline{\mathbf{R}^\varepsilon(\omega, X, X', Z)} \\ \mathbf{R}^\varepsilon(\omega, X, X', Z) & \overline{\mathbf{T}^\varepsilon(\omega, X, X', Z)} \end{pmatrix}, \tag{5.18}$$

with $N \times N$ complex blocks $\mathbf{T}^\varepsilon$ and $\mathbf{R}^\varepsilon$.

5.3. The diffusion limit. The limit of $\mathbf{P}^\varepsilon$ as $\varepsilon \to 0$ is a multidimensional Markov diffusion process, with entries satisfying a system of Itô–Schrödinger equations. This follows from the diffusion approximation theorem [18, 19] (see also [11, sect. 6.3.4]) applied to system (5.8) that we rewrite as

$$\partial_Z \mathbf{P}^\varepsilon(\omega, X, X', Z) = \left[\frac{1}{\varepsilon^{1/2}}\mu\left(X, \frac{Z}{\varepsilon}\right)\mathbf{H}\left(\omega, X, \frac{Z}{\varepsilon^2}\right) + \mathbf{G}\left(\omega, X, \frac{Z}{\varepsilon^2}\right) + \widetilde{\mathbf{K}}^\varepsilon\big(\omega, X, Z\big)\right]\mathbf{P}^\varepsilon(\omega, X, X', Z),$$

$$\mathbf{P}^\varepsilon(\omega, X, X', 0) = \delta(X - X')\mathbf{I}, \tag{5.19}$$

with

$$\begin{aligned}\widetilde{\mathbf{K}}^\varepsilon\big(\omega, X, Z\big) = {}& \big[\mathbf{I} - \mathbf{L}^\varepsilon\big(\omega, X, Z\big)\big]^{-1}\mathbf{L}^\varepsilon\big(\omega, X, Z\big) \\ & \times\left[\frac{1}{\varepsilon^{1/2}}\mu\left(X, \frac{Z}{\varepsilon}\right)\mathbf{H}\left(\omega, X, \frac{Z}{\varepsilon^2}\right) + \mathbf{G}\left(\omega, X, \frac{Z}{\varepsilon^2}\right)\right] \\ & + \big[\mathbf{I} - \mathbf{L}^\varepsilon\big(\omega, X, Z\big)\big]^{-1}\mathbf{K}^\varepsilon\big(\omega, X, Z\big).\end{aligned}$$

The matrix $\widetilde{\mathbf{K}}^\varepsilon$ has the structure

$$\widetilde{\mathbf{K}}^\varepsilon = \begin{pmatrix} \widetilde{\mathbf{K}}^{\varepsilon,a} & \widetilde{\mathbf{K}}^{\varepsilon,b} \\ \overline{\widetilde{\mathbf{K}}^{\varepsilon,b}} & \overline{\widetilde{\mathbf{K}}^{\varepsilon,a}} \end{pmatrix},$$

and its entries are at most of order $\varepsilon^{1/2}$.

Computing the generator of the limit process with the formula given in the diffusion approximation theorem, we obtain that due to the fast phases in the off-diagonal blocks $\mathbf{H}^b$ and $\mathbf{G}^b$ and due to the convergence to zero of $\widetilde{\mathbf{K}}^{\varepsilon,b}$, the complex block $\mathbf{R}^\varepsilon$ converges to zero as $\varepsilon \to 0$. This means that the forward- and backward-going amplitudes decouple as $\varepsilon \to 0$, and this implies that there is no backscattered field in the limit, because the backward-going amplitudes $\boldsymbol{b}^\varepsilon$ are set to zero at $Z = L$. Equation (5.10) simplifies as

$$\boldsymbol{a}^\varepsilon(\omega, X, Z) = \int dX'\, \mathbf{T}^\varepsilon(\omega, X, X', Z)\boldsymbol{a}^\varepsilon(\omega, X', 0), \tag{5.20}$$

where the initial conditions $\boldsymbol{a}^\varepsilon(\omega, X', 0)$ are given in (5.6). The complex matrix $\mathbf{T}^\varepsilon(\omega, X, X', Z)$ is called the transfer process, because it gives the amplitudes of the forward-going modes at positive ranges Z in terms of the initial conditions at $Z = 0$. The limit transfer matrix is described in the next proposition.

PROPOSITION 5.1. *As $\varepsilon \to 0$, $\mathbf{T}^\varepsilon(\omega, X, X', Z)$ converges weakly and in distribution to the diffusion Markov process $\mathbf{T}(\omega, X, X', Z)$. This process is complex and diagonal matrix valued, with diagonal entries $\mathcal{T}_j(\omega, X, X', Z)$ solving the Itô–Schrödinger equations*

$$\begin{aligned} d\mathcal{T}_j(\omega, X, X', Z) = {}& \left[\frac{i}{2\beta_j(\omega)}\partial_X^2 - \frac{q_{jj}^2 R_o(0)}{8\beta_j^2(\omega)}\right]\mathcal{T}_j(\omega, X, X', Z)dZ \\ & + \frac{i\, q_{jj}}{2\beta_j(\omega)}\mathcal{T}_j(\omega, X, X', Z)d\mathcal{B}(X, Z) \end{aligned} \tag{5.21}$$

for $Z > 0$ and initial conditions

$$\mathcal{T}_j(\omega, X, X', 0) = \delta(X - X'), \qquad j = 1, \ldots, N. \tag{5.22}$$

Equations (5.21) *are uncoupled, but they are driven by the same Brownian field* $\mathcal{B}(X,Z)$*, satisfying*

$$\mathbb{E}\left[\mathcal{B}(X,Z)\right]=0, \qquad \mathbb{E}\left[\mathcal{B}(X,Z)\mathcal{B}(X',Z')\right]=\min\{Z,Z'\}R_o(X-X'), \tag{5.23}$$

with R_o *defined in* (3.6)*. Thus, the transfer coefficients* $\mathcal{T}_j$ *are statistically correlated.*

The weak convergence in distribution means that we can calculate the limit $\varepsilon \to 0$ of statistical moments of $\mathbf{T}^\varepsilon$, smoothed by integration over X against the initial conditions, using the Markov diffusion defined by (5.21)–(5.22). In applications we have a fixed $\varepsilon \ll 1$, and we use Proposition 5.1 to approximate the statistical moments of the amplitudes of the forward-going waveguide modes.

The proof of Proposition 5.1 is obtained by the application of the diffusion-approximation theorem [11, sect. 6.3.4]. This theorem states that $\mathbf{T}^\varepsilon$ converges to a diffusion Markov process and it gives the explicit form of the infinitesimal generator. One can then check that this generator is that of the diagonal matrix whose diagonal entries satisfy the Itô–Schrödinger equations (5.21).

When comparing the Itô–Schrödinger equations (5.21) to the deterministic Schrödinger equations (3.15) satisfied by the amplitudes in the ideal waveguides, we see that the random boundary scattering effect amounts to a net diffusion, as described by the last two terms in (5.21). We show next how this leads to loss of coherence of the waves, that is, to exponential decay in range of the mean field. We also study the propagation of energy of the modes and quantify the decorrelation properties of the random fluctuations of their amplitudes.

6. Statistics of the wave field. We begin in section 6.1 with the analysis of the coherent field. Explicitly, we estimate the mean forward-going mode amplitudes in the paraxial long range regime. Traditional imaging methods rely on these being large with respect to their random fluctuations. However, this is not the case, because $\mathbb{E}\left[a_j^\varepsilon(\omega,X,Z)\right]$ decay exponentially with Z, at rates that increase monotonically with mode indices j. The second moments of the amplitudes do not decay, but there is decorrelation over the modes and the frequency and cross-range offsets, as shown in sections 6.3 and 6.4. Understanding these decorrelations is key to designing time reversal and imaging methods that are robust at low SNR. Robust means that wave focusing in time reversal or imaging is essentially independent of the realization of the random boundary fluctuations; it is statistically stable. Low SNR means that the coherent (mean) field, the "signal," is faint with respect to its random fluctuations, the "noise."

6.1. The coherent field. The mean modal amplitudes are

$$\mathbb{E}\left[a_j^\varepsilon(\omega,X,Z)\right] \approx \int dX'\,\mathbb{E}\left[\mathcal{T}_j(\omega,X,X',Z)\right] a_{j,\mathrm{ini}}\left(\omega,X'\right), \tag{6.1}$$

with mean transfer matrix satisfying the partial differential equation

$$\partial_Z \mathbb{E}\left[\mathcal{T}_j(\omega,X,X',Z)\right] = \left[\frac{i}{2\beta_j(\omega)}\partial_X^2 - \frac{1}{\mathcal{S}_j(\omega)}\right]\mathbb{E}\left[\mathcal{T}_j(\omega,X,X',Z)\right], \qquad Z>0, \tag{6.2}$$

with mode-dependent damping coefficients

$$\mathcal{S}_j(\omega)=\frac{8\beta_j^2(\omega)}{q_{jj}^2 R_o(0)}=\frac{2\mathcal{D}^2}{\sigma^2\pi^2\ell}\left[\frac{(N+\alpha(\omega)-1/2)^2-(j-1/2)^2}{(j-1/2)^4}\right], \tag{6.3}$$

with units of length. Here we used definitions (2.13), (2.14), and (3.9) and obtained (6.3) by taking expectations in (5.21). Its solution is given by

$$\mathbb{E}\left[\mathcal{T}_j(\omega,X,X',Z)\right] = \sqrt{\frac{\beta_j(\omega)}{2\pi i Z}}\exp\left[-\frac{Z}{\mathcal{S}_j(\omega)} + \frac{i\beta_j(\omega)(X-X')^2}{2Z}\right], \tag{6.4}$$

and the mean modal amplitudes are obtained from (6.1) and (5.6),

$$\begin{aligned}\mathbb{E}\left[a_j^\varepsilon(\omega,X,Z)\right] &\approx -\frac{1}{2}\sqrt{\frac{i}{2\pi\beta_j(\omega)Z}}\int dX'\,\widehat{F}_j(\omega,X') \\ &\quad\times\exp\left[-\frac{Z}{\mathcal{S}_j(\omega)} + \frac{i\beta_j(\omega)(X-X')^2}{2Z}\right] \\ &= a_{j,o}\left(\omega,X,Z\right)\exp\left[-\frac{Z}{\mathcal{S}_j(\omega)}\right], \end{aligned} \tag{6.5}$$

with $a_{j,o}$ the solution of the paraxial wave equation (3.15)–(3.16) in the ideal waveguide.

The mean wave field follows from (4.6), after neglecting the evanescent part,

$$\mathbb{E}\left[\widehat{P}\left(\omega,\frac{X}{\varepsilon},\eta,\frac{Z}{\varepsilon^2}\right)\right] \approx \sum_{j=1}^N \phi_j(\eta)a_{j,o}\left(\omega,X,Z\right)\exp\left[-\frac{Z}{\mathcal{S}_j(\omega)} + i\beta_j(\omega)\frac{Z}{\varepsilon^2}\right]. \tag{6.6}$$

It is different from the field in the ideal waveguides,

$$\widehat{p}_o\left(\omega,\frac{X}{\varepsilon},\eta,\frac{Z}{\varepsilon^2}\right) \approx \sum_{j=1}^N \phi_j(\eta)a_{j,o}\left(\omega,X,Z\right)\exp\left[i\beta_j(\omega)\frac{Z}{\varepsilon^2}\right], \tag{6.7}$$

because of the exponential decay of the mean mode amplitudes, on range scales $\mathcal{S}_j(\omega)$.

6.2. High-frequency and low-SNR regime. We call the length scales $\mathcal{S}_j(\omega)$ the *mode-dependent scattering mean free paths*, because they give the range over which the modes become essentially incoherent, with low SNR,

$$\mathrm{SNR}_{j,\omega} = \frac{\left|\mathbb{E}\left[a_j^\varepsilon(\omega,X,Z)\right]\right|}{\sqrt{\mathbb{E}\left[|a_j^\varepsilon(\omega,X,Z)|^2\right] - \left|\mathbb{E}\left[a_j^\varepsilon(\omega,X,Z)\right]\right|^2}} \sim \exp\left[-\frac{Z}{\mathcal{S}_j(\omega)}\right] \ll 1 \quad \text{if } Z \gg \mathcal{S}_j(\omega). \tag{6.8}$$

The second moments $\mathbb{E}\left[|a_j^\varepsilon(\omega,X,Z)|^2\right]$ are calculated in the next section, and they do not decay with range. This is why (6.8) holds.

The scattering mean free paths decrease monotonically with mode indices j, as shown in (6.3). The first mode encounters less often the random boundary and has the longest scattering mean free path

$$\mathcal{S}_1(\omega) = \frac{32\mathcal{D}^2}{\sigma^2\pi^2\ell}\left[(N+\alpha(\omega)-1/2)^2 - 1/4\right] \approx \frac{32\mathcal{D}^2N^2}{\sigma^2\pi^2\ell}. \tag{6.9}$$

The highest indexed mode scatters most frequently at the boundary, and its scattering mean free path

$$\mathcal{S}_N(\omega) = \frac{2\mathcal{D}^2}{\sigma^2\pi^2\ell}\frac{\alpha(\omega)\left(2N+\alpha(\omega)-1\right)}{(N-1/2)^4} \approx \frac{\alpha(\omega)}{8}\frac{\mathcal{S}_1(\omega)}{N^5} \tag{6.10}$$

is much smaller than $\mathcal{S}_1(\omega)$ when N is large. To be complete, we also have

$$\mathcal{S}_j(\omega) \approx \mathcal{S}_1(\omega)\frac{1-s^4}{s^4}\frac{1}{N^4} \qquad \text{if } j = \lfloor sN \rfloor, \quad s \in (0,1),$$

and

$$\mathcal{S}_j(\omega) \approx \mathcal{S}_1(\omega)\frac{1}{(2j-1)^4} \qquad \text{if } j = o(N).$$

Our analysis of time reversal and imaging is carried in a high-frequency regime, with waveguide depth $\mathcal{D}$ larger than the central wavelength λ_o or, equivalently, with $N \gg 1$. We also assume a low-SNR regime, with scaled range Z exceeding the scattering mean free path of all the modes, so that none of the amplitudes a_j is coherent. This is the most challenging case for sensor array imaging, because the wave field measured at the sensors is dominated by noise. We model the low-SNR regime using the dimensionless large parameter

$$\gamma = \frac{Z}{\mathcal{S}_1(\omega_0)} \gg 1 \tag{6.11}$$

and observe from (6.3) that

$$\frac{Z}{\mathcal{S}_j(\omega_0)} \geq \gamma \gg 1 \quad \text{for all } j = 1, \ldots, N. \tag{6.12}$$

6.3. The second moments. The quantification of SNR and the analysis of time reversal and imaging involves the second moments of the mode amplitudes. Recall that

$$a_j^\varepsilon(\omega, X, Z) \approx \int dX' \mathcal{T}_j^\varepsilon(\omega, X, X', Z)\, a_{j,\mathrm{ini}}(\omega, X'), \tag{6.13}$$

with $\mathcal{T}_j^\varepsilon$ the diagonal entries of the transfer matrix $\mathbf{T}^\varepsilon$. To calculate the second moments, we estimate $\mathbb{E}\left[\mathcal{T}_j^\varepsilon \overline{\mathcal{T}_l^\varepsilon}\right]$. The equations for $\mathcal{T}_j^\varepsilon(\omega_1, X_1, X_1', Z)\overline{\mathcal{T}_l^\varepsilon(\omega_2, X_2, X_2', Z)}$ follow[2] from the forward scattering approximation of (5.8),

$$\begin{aligned}\partial_Z \mathcal{T}_j^\varepsilon \overline{\mathcal{T}_l^\varepsilon} \approx{}& \left[\frac{i}{2\beta_j(\omega_1)}\partial_{X_1}^2 - \frac{i}{2\beta_l(\omega_2)}\partial_{X_2}^2\right]\mathcal{T}_j^\varepsilon \overline{\mathcal{T}_l^\varepsilon} \\ &- \frac{i}{2\varepsilon^{1/2}}\left[\frac{q_{jj}\,\mu(X_1, Z/\varepsilon)}{\beta_j(\omega_1)} - \frac{q_{ll}\,\mu(X_2, Z/\varepsilon)}{\beta_l(\omega_2)}\right]\mathcal{T}_j^\varepsilon \overline{\mathcal{T}_l^\varepsilon}\end{aligned} \tag{6.14}$$

for $Z > 0$, with initial condition

$$\mathcal{T}_j^\varepsilon(\omega_1, X_1, X_1', 0)\overline{\mathcal{T}_l^\varepsilon(\omega_2, X_2, X_2', 0)} = \delta(X_1 - X_1')\delta(X_2 - X_2'). \tag{6.15}$$

Their statistical distribution is characterized in the limit $\varepsilon \to 0$ by the diffusion approximation theorem [18, 19]; see also [11, Chap. 6]. It is the distribution of $\mathcal{T}_j(\omega_1, X_1, Z)\overline{\mathcal{T}_l}(\omega_2, X_2, Z)$, with $\mathcal{T}_j$ the limit transfer coefficients in Proposition 5.1. This gives the approximate relation

$$\begin{aligned}\mathbb{E}\left[a_j^\varepsilon(\omega_1, X_1, Z)\overline{a_l^\varepsilon(\omega_2, X_2, Z)}\right] \approx{}& \int dX_1' \int dX_2'\, a_{j,\mathrm{ini}}(\omega_1, X_1')\,\overline{a_{l,\mathrm{ini}}(\omega_2, X_2')} \\ &\times \mathbb{E}\left[\mathcal{T}_j(\omega_1, X_1, X_1', Z)\overline{\mathcal{T}_l(\omega_2, X_2, X_2', Z)}\right].\end{aligned} \tag{6.16}$$

The calculation of $\mathbb{E}\left[\mathcal{T}_j\overline{\mathcal{T}_l}\right]$ is given in Appendix A. We summarize the results in Propositions 6.1–6.3.

[2]Here we neglected the higher-order terms that play no role in the limit $\varepsilon \to 0$.

6.3.1. The single mode and frequency moments. It is easier to calculate the diagonal moments, with $j = l$, and the same frequency $\omega_1 = \omega_2 = \omega$. We have the following result proved in Appendix A.

PROPOSITION 6.1. *For all $j = 1, \ldots, N$ and all the frequencies $\omega \in [\omega_0 - B/2, \omega_0 + B/2]$,*

$$\begin{aligned}
&\mathbb{E}\left[\mathcal{T}_j(\omega, X_1, X_1', Z)\overline{\mathcal{T}_j(\omega, X_2, X_2', Z)}\right] \\
&= \frac{\beta_j(\omega)}{2\pi Z} \exp\left\{\frac{i\beta_j(\omega)[(X_1 - X_1')^2 - (X_2 - X_2')^2]}{2Z}\right. \\
&\qquad \left. - \frac{2Z}{\mathcal{S}_j(\omega)} \int_0^1 ds\, C_o\big[(X_1 - X_2)s + (X_1' - X_2')(1-s)\big]\right\}, \qquad (6.17)
\end{aligned}$$

with kernel C_o defined by

$$C_o(X) = 1 - \frac{R_o(X)}{R_o(0)}. \qquad (6.18)$$

The general second moment formula does not have an explicit form in arbitrary regimes. But it can be approximated in the low-SNR regime (6.11). The expression (6.17) also simplifies in that regime, as stated in the following proposition, which we prove below.

PROPOSITION 6.2. *In the low-SNR regime* (6.11) *and under the assumption $X_1' = X_2' = X'$, the right-hand side in* (6.17) *is essentially zero, unless*

$$\frac{|X_1 - X_2|}{\ell} \lesssim \sqrt{\frac{3\,\mathcal{S}_j(\omega)}{\gamma\,\mathcal{S}_1(\omega)}} \ll 1, \qquad (6.19)$$

and the moment formula simplifies to

$$\begin{aligned}
&\mathbb{E}\left[\mathcal{T}_j(\omega, X_1, X', Z)\overline{\mathcal{T}_j(\omega, X_2, X', Z)}\right] \\
&\approx \frac{\beta_j}{2\pi Z} \exp\left[\frac{i\beta_j[(X_1 - X')^2 - (X_2 - X')^2]}{2Z} - \frac{(X_1 - X_2)^2}{2X_{d,j}^2(\omega)}\right], \qquad (6.20)
\end{aligned}$$

with

$$X_{d,j}(\omega) = \ell\sqrt{\frac{3\,\mathcal{S}_j(\omega)}{2Z}} = \ell\sqrt{\frac{3\,\mathcal{S}_j(\omega)}{2\gamma\,\mathcal{S}_1(\omega)}} \ll \ell. \qquad (6.21)$$

If the initial points X_1' and X_2' are different, but still close enough to satisfy

$$\frac{|X_1' - X_2'|}{\ell} \ll 1, \qquad (6.22)$$

the moment formula becomes

$$\begin{aligned}
\mathbb{E}\left[\mathcal{T}_j(\omega, X_1, X_1', Z)\overline{\mathcal{T}_j(\omega, X_2, X_2', Z)}\right] &\approx \frac{\beta_j}{2\pi Z} \exp\left[\frac{i\beta_j[(X_1 - X_2')^2 - (X_2 - X_2')^2]}{2Z}\right] \\
&\times \exp\left[-\frac{(X_1 - X_2)^2 + (X_1' - X_2')^2 + (X_1 - X_2)(X_1' - X_2')}{2X_{d,j}^2(\omega)}\right]. \qquad (6.23)
\end{aligned}$$

Proof. We see from definitions (3.6) and (6.18) that $C_o(X) \approx 1$ for $|X| \gg \ell$. Therefore,

$$\int_0^1 ds\, C_o\big[(X_1 - X_2)s\big] \approx 1 \quad \text{if } |X_1 - X_2| \gg \ell,$$

and the right-hand side in (6.17) becomes negligible, of order $O\left(e^{-2Z/\mathcal{S}_j}\right) \ll 1$. In the case $|X_1 - X_2| \sim \ell$ we obtain similarly that the damping term is of order Z, and the right-hand side in (6.17) is exponentially small. It is only when $|X_1 - X_2| \ll \ell$ that the moment does not vanish. Then, we can approximate the kernel C_o in the integral with its first nonzero term in the Taylor expansion around zero, using the relations

$$C_o(0) = 0, \quad C_o'(0) = 0, \quad \text{and } C_o''(0) = -\frac{R_o''(0)}{R_o(0)} = \frac{1}{\ell^2}, \tag{6.24}$$

that follow from (3.9)–(3.7). We have

$$\int_0^1 ds\, C_o\big[(X_1 - X_2)s\big] \approx \frac{|X_1 - X_2|^2}{6\ell^2} \quad \text{if } |X_1 - X_2| \gg \ell,$$

and the right-hand side in (6.17) is of the order $\exp[-\frac{|X_1 - X_2|^2 Z}{3\ell^2 \mathcal{S}_j}]$. This gives the condition (6.19), and the simpler moment formula (6.20) follows.

Essentially the same proof applies in the case $X_1' \neq X_2'$, because we can still expand the integrand in (6.17) by assumption (6.22). ∎

6.3.2. The two mode and frequency moments. The general second moment formula is derived in Appendix A, in the low-SNR regime (6.11). It has a complicated expression that we do not repeat here, but it simplifies for nearby frequencies, as stated below.

PROPOSITION 6.3. *The modes decorrelate under the low-SNR assumption* (6.11):

$$\mathbb{E}\left[\mathcal{T}_j\left(\omega_1, X_1, X_1', Z\right)\overline{\mathcal{T}_l\left(\omega_2, X_2, X_2', Z\right)}\right] \approx 0 \quad \textit{if } j \neq l \tag{6.25}$$

for any two frequencies ω_1, ω_2 and cross-ranges X_1, X_2. The modes also decorrelate for frequency offsets that exceed

$$\Omega_{d,j}(\omega) = \frac{\mathcal{S}_j(\omega)\beta_j^2(\omega)\ell^2}{Z^2|\beta_j'(\omega)|} = \frac{\beta_j(\omega)}{|\beta_j'(\omega)|}\frac{\mathcal{S}_j(\omega)\beta_j(\omega)\ell^2}{\gamma^2\mathcal{S}_1^2(\omega)}, \tag{6.26}$$

where $\beta_j'(\omega)$ is the derivative of $\beta_j(\omega)$ with respect to ω. For much smaller frequency offsets satisfying

$$|\omega_1 - \omega_2| \ll \Omega_{d,j}\left(\omega\right), \quad \omega = \frac{\omega_1 + \omega_2}{2}, \tag{6.27}$$

the moment formula is

$$\begin{aligned}\mathbb{E}\left[\mathcal{T}_j\left(\omega_1, X_1, X_1', Z\right)\overline{\mathcal{T}_j\left(\omega_2, X_2, X_2', Z\right)}\right] &\approx \frac{\beta_j(\omega)}{2\pi Z} \\ \times \exp\Bigg\{&\frac{i\left[\beta_j(\omega_1)(X_1 - X_1')^2 - \beta_j(\omega_2)(X_2 - X_2')^2\right]}{2Z} \\ &- \frac{(X_1 - X_2)^2 + (X_1' - X_2')^2 + (X_1 - X_2)(X_1' - X_2')}{2X_{d,j}^2(\omega)}\Bigg\}.\end{aligned} \tag{6.28}$$

6.4. Decorrelation properties. We already stated the decorrelation of the modes in Proposition 6.3. But even for a single mode, we have decorrelation over cross-range and frequency offsets.

The *decoherence length* of mode j is denoted by $X_{d,j}(\omega)$, and it is defined in (6.21). It is the length scale over which the second moment at frequency ω decays with cross-range. It follows from (6.21) that $X_{d,j}$ is much smaller than the correlation length, for all the modes, and that it decreases monotonically with j. The first mode has the largest decorrelation length

$$X_{d,1}(\omega) = \ell\sqrt{\frac{3}{2\gamma}}, \tag{6.29}$$

because it scatters less often at the boundary. The decoherence length of the highest mode is much smaller in high-frequency regimes with $N \gg 1$,

$$X_{d,N}(\omega) = X_{d,1}(\omega)\sqrt{\frac{\mathcal{S}_N(\omega)}{\mathcal{S}_1(\omega)}} \approx \frac{\ell}{8}\sqrt{\frac{3\alpha(\omega)}{\gamma}}N^{-5/2}. \tag{6.30}$$

The decorrelation frequency is derived in Appendix A.2. It is given by (6.26) or, more explicitly, by

$$\Omega_{d,j}(\omega) \approx \frac{\omega\sigma^2\pi^3}{64\gamma^2}\left(\frac{\ell}{\lambda}\right)^3 \frac{\left[\left(N+\alpha(\omega)-\frac{1}{2}\right)^2 - \left(j-\frac{1}{2}\right)^2\right]^{5/2}}{N^9(j-1/2)^4}, \tag{6.31}$$

it is much smaller than ω for all the modes, and it decreases monotonically with j, starting from

$$\Omega_{d,1}(\omega) \approx \frac{\omega\sigma^2\pi^3(\ell/\lambda)^3}{4\gamma^2N^4}. \tag{6.32}$$

7. The forward model. Let us gather the results and summarize them in the following model of the pressure field:

$$\widehat{P}\left(\omega, \frac{X}{\varepsilon}, \eta, \frac{Z}{\varepsilon^2}\right) \approx \sum_{j=1}^{N} \frac{\phi_j(\eta)}{2i\beta_j(\omega)} e^{i\beta_j(\omega)\frac{Z}{\varepsilon^2}} \int dX'\, \mathcal{T}_j(\omega, X, X', Z) \int_0^{\mathcal{D}} d\eta'\phi_j(\eta')\, \widehat{f}(\omega, X', \eta'), \tag{7.1}$$

where the symbol $\approx$ stands for approximate, in distribution. That is to say, the statistical moments of the random pressure field $\widehat{P}$ are equal to those of the right-hand side in the limit $\varepsilon \to 0$. The first and second moments follow from Propositions 5.1–6.3. In our analysis of time reversal and imaging we take small frequency offsets, satisfying $|\widetilde{\omega}| \ll \Omega_{d,j}(\omega)$, so that we can use the simpler moment formula (6.28).

The computation of the fourth moments of the transfer coefficients is quite involved. We estimate some of them in Appendix B for a particular combination of the mode indices and arguments. These moments are used in the next sections to show the statistical stability of the time reversal and coherent interferometric imaging functions.

We analyze next time reversal and imaging in the low-SNR regime defined in section 6.2. We assume for convenience that the source (3.1) has the separable form

$$f(t, X, \eta) = \frac{\mathfrak{f}(t)}{\theta_X\theta_\eta}\rho\left(\frac{X - X^\star}{\theta_X}, \frac{\eta - \eta^\star}{\theta_\eta}\right), \tag{7.2}$$

meaning that the same pulse $\mathfrak{f}(t)$ is emitted from all the points in the support of the nonnegative source density ρ. We scale this support with the dimensionless parameters θ_X and θ_η and normalize the source by

$$\int \frac{dX'}{\theta_X} \int \frac{d\eta'}{\theta_\eta} \rho\left(\frac{X - X^\star}{\theta_X}, \frac{\eta - \eta^\star}{\theta_\eta}\right) = 1. \tag{7.3}$$

To analyze the resolution of time reversal and imaging, we study in detail the case of a source density localized around the point $(X^\star, \eta^\star, 0)$. In an abuse of terminology we may say that we study the "point spread" time reversal and imaging functions, because $f(t, X, \eta)$ has small support. Note, however, that it is not a point source. Recalling the definition (3.1), we see that $f(t, X, \eta)$ is the source after the cross-range scaling by ε. The actual source has cross-range support θ_X/ε and θ_η, with positive parameters θ_X and θ_η that are small but independent of ε.

The coefficients

$$\widehat{F}_j(\omega, X) = \frac{\widehat{\mathfrak{f}}(\omega)}{\theta_X \theta_\eta} \int_0^{\mathcal{D}} d\eta\, \phi_j(\eta) \rho\left(\frac{X - X^\star}{\theta_X}, \frac{\eta - \eta^\star}{\theta_\eta}\right) \tag{7.4}$$

are proportional to the Fourier coefficients $\widehat{\mathfrak{f}}(\omega)$ of the pulse and are thus supported in the frequency interval $[\omega_o - B/2, \omega_o + B/2]$. We write this explicitly by letting

$$\mathfrak{f}(t) = e^{-i\omega_o t} \varphi(Bt), \qquad \widehat{\mathfrak{f}}(\omega) = B^{-1} \widehat{\varphi}\left(\frac{\omega - \omega_o}{B}\right), \tag{7.5}$$

with function φ of dimensionless arguments and Fourier transform $\widehat{\varphi}$ supported in the interval $[-1/2, 1/2]$. The pulse $\mathfrak{f}(t)$ is large in a time interval proportional to B, and we distinguish two regimes: the *broadband* regime with $B \gg \varepsilon^2 \omega_o$, and the *narrowband* regime with $B \leq \varepsilon^2 \omega_o$. The comparison with ε^2 is because the source is at range $Z_{\mathcal{A}}/\varepsilon^2$ from the array, and the modes arrive at time intervals of order $1/\varepsilon^2$. Broadband pulses have smaller support than these travel times, meaning that we can observe the different arrivals of the modes, at least in the ideal waveguides. In any case, we assume that $B \ll \omega_o$ so that we can fix the number of propagating modes to that at the central frequency, as explained in section 2.

8. Time reversal. Let us denote by $D(t, X, \eta)$ the pressure field measured in a time window $\psi(t/T^\varepsilon)$ at an array $\mathcal{A}$, with aperture modeled by the indicator function

$$1_{\mathcal{A}}(X, \eta) = 1_{\mathcal{A}_X}(X) 1_{\mathcal{A}_\eta}(\eta), \tag{8.1}$$

at range $z_{\mathcal{A}} = Z_{\mathcal{A}}/\varepsilon^2$. Here X is the scaled cross-range in the array, related to the cross-range x by $x = X/\varepsilon$, and $\mathcal{A}_X \subset \mathbb{R}$ and $\mathcal{A}_\eta \subset [0, \mathcal{D}]$ are intervals in X and η. The window ψ is a function of dimensionless arguments, of support of order one, and T^ε denotes the length of time of the measurements. Because the waves travel distances of order ε^{-2}, we scale T^ε as $T^\varepsilon = T/\varepsilon^2$, with T of order one.

In time reversal the array takes the recorded field $D(t, X, \eta)$, time reverses it, and emits $D(T^\varepsilon - t, X, \eta)$ back in the medium. We study in this section the resolution of the refocusing of the waves at the source, in the high-frequency and low-SNR regime described in section 6.2. We compare the results with those in ideal waveguides, to show the improved refocusing in random waveguides. The resolution analysis includes that of statistical stability, which quantifies the robustness of the refocusing with respect to different realizations of the random boundary fluctuations.

8.1. Mathematical model of time reversal. We have in our notation

$$D(t,X,\eta) = 1_{\mathcal{A}}(X,\eta)\psi\left(\frac{t}{T^\varepsilon}\right)P\left(t, x=\frac{X}{\varepsilon}, \eta, z_{\mathcal{A}}=\frac{Z_{\mathcal{A}}}{\varepsilon^2}\right), \tag{8.2}$$

with mathematical model following from (7.1),

$$\begin{aligned} D(t,X,\eta) &\approx 1_{\mathcal{A}}(X,\eta)\psi\left(\frac{t}{T^\varepsilon}\right)\sum_{j=1}^N \phi_j(\eta) \\ &\times \int d\omega\, \frac{e^{i\beta_j(\omega)\frac{Z_{\mathcal{A}}}{\varepsilon^2}-i\omega t}}{2i\beta_j(\omega)} \int dX'\, \widehat{F}_j(\omega,X')\mathcal{T}_j(\omega,X,X',Z_{\mathcal{A}}). \end{aligned} \tag{8.3}$$

The time-reversed field $D^{\rm TR}$ and its Fourier transform are given by

$$D^{\rm TR}(t,X,\eta) = D(T^\varepsilon - t, X, \eta)\,, \qquad \widehat{D}^{\rm TR}(\omega,X,\eta) = e^{i\omega T^\varepsilon}\overline{\widehat{D}(\omega,X,\eta)}\,, \tag{8.4}$$

with

$$\begin{aligned} \widehat{D}(\omega,X,\eta) &\approx 1_{\mathcal{A}}(X,\eta)\sum_{j=1}^N \phi_j(\eta)\int \frac{du}{2\pi}\,\widehat{\psi}(u)\frac{e^{i\beta_j(\omega-\varepsilon^2u/T)\frac{Z_{\mathcal{A}}}{\varepsilon^2}}}{2i\beta_j(\omega-\varepsilon^2u/T)} \\ &\times \int dX'\,\widehat{F}_j\left(\omega-\frac{\varepsilon^2u}{T},X'\right)\mathcal{T}_j\left(\omega-\frac{\varepsilon^2u}{T},X,X',Z_{\mathcal{A}}\right). \end{aligned} \tag{8.5}$$

The small frequency shifts ε^2u/T are due to the time scaling, and we can neglect them in the source terms $\widehat{F}_j$ and in the argument of the amplitude factor $1/\beta_j$.

We are interested in the wave at the range of the source, observed at coordinates $(x^s = X^s/\varepsilon, \eta^s, z^s = 0)$. We can model it by

$$\begin{aligned} \mathcal{O}(t,X^s,\eta^s) &= \sum_{j=1}^N \phi_j(\eta^s)\int \frac{d\omega}{2\pi}\,\frac{e^{i\beta_j(\omega)\frac{Z_{\mathcal{A}}}{\varepsilon^2}-i\omega t}}{2i\beta_j(\omega)} \\ &\times \int dX \int d\eta\,\phi_j(\eta)\,\widehat{D}^{\rm TR}(\omega,X,\eta)\,\mathcal{T}_j(\omega,X,X^s,Z_{\mathcal{A}}), \end{aligned}$$

using reciprocity. Note the similarity with (7.1), except that the source is now at the array, which we approximate as a continuum, instead of a discrete collection of sensors. This approximation is convenient for the analysis, because sums over the sensors are replaced by integrals over the X and η apertures, of lengths $|\mathcal{A}_X|$ and $|\mathcal{A}_\eta|$. We assume henceforth that

$$\mathcal{A}_X = \left[-\frac{|\mathcal{A}_X|}{2},\frac{|\mathcal{A}_X|}{2}\right], \qquad \mathcal{A}_\eta = [\eta_1,\eta_2] \subset [0,\mathcal{D}] \tag{8.6}$$

and define the matrix

$$\Gamma_{jl} = \int_0^{\mathcal{D}} d\eta\, 1_{\mathcal{A}_\eta}(\eta)\,\phi_j(\eta)\phi_l(\eta) \tag{8.7}$$

that models the coupling of the modes in the expression of refocused field, due to a finite aperture. It becomes the identity when the array has full aperture $\mathcal{A}_\eta = [0,\mathcal{D}]$.

Using (8.4) in the expression of $\mathcal{O}$ we obtain

$$\begin{aligned}\mathcal{O}(t,X^s,\eta^s) \approx & \int \frac{dX'}{\theta_X}\int \frac{d\eta'}{\theta_\eta}\,\rho\left(\frac{X'-X^\star}{\theta_X},\frac{\eta'-\eta^\star}{\theta_\eta}\right)\sum_{j,l=1}^{N}\Gamma_{jl}\\ &\times\int\frac{du}{2\pi}\,\overline{\widehat{\psi}(u)}\int\frac{d\omega}{2\pi}\,\overline{\widehat{\mathfrak{f}}(\omega)}\,\frac{\phi_j(\eta^s)\phi_l(\eta')}{4\beta_j(\omega)\beta_l(\omega)}\\ &\times e^{i\omega(T^\varepsilon-t)+i\beta_j(\omega)\frac{Z_{\mathcal{A}}}{\varepsilon^2}-i\beta_l(\omega-\frac{\varepsilon^2 u}{T})\frac{Z_{\mathcal{A}}}{\varepsilon^2}}\\ &\times\int_{-|\mathcal{A}_X|/2}^{|\mathcal{A}_X|/2}dX\,\mathcal{T}_j\Big(\omega,X,X^s,Z_{\mathcal{A}}\Big)\overline{\mathcal{T}_l\Big(\omega-\frac{\varepsilon^2u}{T},X,X',Z_{\mathcal{A}}\Big)}.\end{aligned}$$

Moreover, assuming a tightly supported source density around $(X^\star,\eta^\star)$, modeled by small θ_X and θ_η, and recalling that the bandwidth B of $\widehat{\mathfrak{f}}(\omega)$ satisfies $B\ll\omega_o$, we can simplify the result as

$$\begin{aligned}\mathcal{O}(t,X^s,\eta^s)\approx & \sum_{j,l=1}^{N}\Gamma_{jl}\frac{\phi_j(\eta^s)\phi_l(\eta^\star)}{4\beta_j(\omega_o)\beta_l(\omega_o)}\,\psi\left(\frac{\beta_l'(\omega_o)Z_{\mathcal{A}}}{T}\right)\\ &\times\int\frac{d\omega}{2\pi}\,\overline{\widehat{\mathfrak{f}}(\omega)}e^{i\omega(T^\varepsilon-t)+i[\beta_j(\omega)-\beta_l(\omega)]\frac{Z_{\mathcal{A}}}{\varepsilon^2}}\\ &\times\int_{-|\mathcal{A}_X|/2}^{|\mathcal{A}_X|/2}dX\,\mathcal{T}_j\Big(\omega,X,X^s,Z_{\mathcal{A}}\Big)\overline{\mathcal{T}_l\Big(\omega,X,X^\star,Z_{\mathcal{A}}\Big)}.\end{aligned}\tag{8.8}$$

Here we used the differentiability of $\mathcal{T}_l$ with respect to the frequency argument, which is not difficult to deduce using the type of analysis described in section 5.3, and evaluated the integral over u, the inverse Fourier transform of the recording window ψ. Note that $\beta_l'(\omega_o)Z_{\mathcal{A}}$ are the scaled travel times of the waveguide modes, so only the first N_T modes that arrive within the time support of the window ψ contribute in (8.8). They satisfy

$$\beta_l'(\omega_o)Z_{\mathcal{A}}\le T,\qquad l=1,\dots,N_T.\tag{8.9}$$

8.2. Time reversal in ideal waveguides. The observed wavefield in ideal waveguides follows from (8.8) and the expression

$$\mathcal{T}_{j,o}(\omega,X,X',Z)=\sqrt{\frac{\beta_j(\omega)}{2\pi iZ}}\exp\left[\frac{i\beta_j(\omega)(X-X')^2}{2Z}\right]\tag{8.10}$$

of the ideal transfer coefficients, defined by the Green's functions of the paraxial operator in (3.15). We obtain that

$$\begin{aligned}\mathcal{O}_o(t,X^s,\eta^s)\approx & \frac{|\mathcal{A}_X|}{8\pi Z_{\mathcal{A}}}\sum_{j=1}^{N}\sum_{l=1}^{N_T}\Gamma_{jl}\frac{\phi_j(\eta^s)\phi_l(\eta^\star)}{4\sqrt{\beta_j(\omega_o)\beta_l(\omega_o)}}\\ &\times\int_{-|\mathcal{A}_X|/2}^{|\mathcal{A}_X|/2}\frac{dX}{|\mathcal{A}_X|}e^{\frac{i\beta_j(\omega_o)(X-X^s)^2}{2Z_{\mathcal{A}}}-\frac{i\beta_l(\omega_o)(X-X^\star)^2}{2Z_{\mathcal{A}}}}\\ &\times\int\frac{dh}{2\pi}\,\overline{\widehat{\varphi}(h)}\,e^{i\left[\beta_j(\omega_o+Bh)-\beta_l(\omega_o+Bh)\right]\frac{Z_{\mathcal{A}}}{\varepsilon^2}+i(\omega_o+Bh)(T^\varepsilon-t)},\end{aligned}\tag{8.11}$$

where we used the definition (7.5) of the emitted pulse and the assumption $B\ll\omega_o$.

The refocusing of $\mathcal{O}_o$ depends on the bandwidth. If the emitted signal is broadband, with $B \gg \varepsilon^2\omega_o$, then we see a refocused pulse at the discrete set of observation times

$$t^\varepsilon_{jl} = t_{j,l}/\varepsilon^2, \qquad t_{j,l} = T + [\beta'_j(\omega_o) - \beta'_l(\omega_o)]Z_{\mathcal{A}}.$$

Only one term of the sum in (8.11) contributes at time $t^\varepsilon_{j,l}$ for $j \neq l$, so there is no refocusing in the depth coordinate η. The refocusing in cross-range is dictated by the Fresnel-type integral in X, which peaks at search locations

$$X^s = \frac{\beta_l(\omega_o)}{\beta_j(\omega_o)} X^\star \neq X^\star.$$

The wave field refocuses at the source only at time T^ε, corresponding to $j = l$ above, where all the diagonal terms contribute to the sum in (8.11). Thus, we define the time reversal function as

$$\mathcal{J}_o^{\mathrm{TR,bb}}(X^s, \eta^s) = \mathcal{O}_o(T^\varepsilon, X^s, \eta^s), \tag{8.12}$$

where the index "bb" stands for broadband, and obtain that

$$\begin{aligned}\mathcal{J}_o^{\mathrm{TR,bb}}(X^s, \eta^s) \approx{}& \frac{|\mathcal{A}_X|\,\overline{\varphi}(0)}{8\pi Z_{\mathcal{A}}} \sum_{j=1}^{N_T} \Gamma_{jj} \frac{\phi_j(\eta^s)\phi_j(\eta^\star)}{4\beta_j(\omega_o)} \\ &\times e^{i\beta_j(\omega_o)\frac{[(X^s)^2 - (X^\star)^2]}{2Z_{\mathcal{A}}}} \operatorname{sinc}\left[\frac{\beta_j(\omega_o)(X^\star - X^s)|\mathcal{A}_X|}{2Z_{\mathcal{A}}}\right],\end{aligned} \tag{8.13}$$

where $\operatorname{sinc}(s) = \sin(s)/s$. This function is focused at $X^s = X^\star$ and $\eta^s = \eta^\star$, as we discuss in more detail in section 8.4, where we compare the resolution with that in random waveguides.

If the emitted signal is narrowband, say with $B = \varepsilon^2\mathfrak{B}$ and scaled bandwidth $\mathfrak{B}$ of order ω_o, we can rewrite (8.11) as

$$\begin{aligned}\mathcal{O}_o(t, X^s, \eta^s) \approx{}& \frac{|\mathcal{A}_X|}{8\pi Z_{\mathcal{A}}} \sum_{j=1}^{N} \sum_{l=1}^{N_T} \Gamma_{jl} \frac{\phi_j(\eta^s)\phi_l(\eta^\star)}{4\sqrt{\beta_j(\omega_o)\beta_l(\omega_o)}} \\ &\times \int_{-|\mathcal{A}_X|/2}^{|\mathcal{A}_X|/2} \frac{dX}{|\mathcal{A}_X|} e^{\frac{i\beta_j(\omega_o)(X-X^s)^2}{2Z_{\mathcal{A}}} - \frac{i\beta_l(\omega_o)(X-X^\star)^2}{2Z_{\mathcal{A}}}} \\ &\times e^{i\left[\beta_j(\omega_o) - \beta_l(\omega_o)\right]\frac{Z_{\mathcal{A}}}{\varepsilon^2} + i\omega_o(T^\varepsilon - t)}\,\overline{\varphi} \\ &\times \left[\mathfrak{B}(T - \varepsilon^2 t) + \mathfrak{B}(\beta'_j(\omega_o) - \beta'_l(\omega_o))Z_{\mathcal{A}}\right].\end{aligned} \tag{8.14}$$

Here all the terms contribute to the sum, but we have oscillations over the index offsets $j - l$, due to the $O(\varepsilon^{-2})$ phase of the exponential. Thus, we expect that the leading contribution comes from the diagonal terms in (8.14), which refocus around the time $t = T^\varepsilon$. The narrowband time reversal function, defined as above by $\mathcal{O}_o(T^\varepsilon, X^s, \eta^s)$, is

$$\begin{aligned}\mathcal{J}_o^{\mathrm{TR,nb}}(X^s, \eta^s) \approx{}& \frac{|\mathcal{A}_X|}{8\pi Z_{\mathcal{A}}} \sum_{j=1}^{N} \sum_{l=1}^{N_T} \Gamma_{jl} \frac{\phi_j(\eta^s)\phi_l(\eta^\star)}{4\sqrt{\beta_j(\omega_o)\beta_l(\omega_o)}} \\ &\times \int_{-|\mathcal{A}_X|/2}^{|\mathcal{A}_X|/2} \frac{dX}{|\mathcal{A}_X|} e^{\frac{i\beta_j(\omega_o)(X-X^s)^2}{2Z_{\mathcal{A}}} - \frac{i\beta_l(\omega_o)(X-X^\star)^2}{2Z_{\mathcal{A}}}} \\ &\times e^{i\left[\beta_j(\omega_o) - \beta_l(\omega_o)\right]\frac{Z_{\mathcal{A}}}{\varepsilon^2}}\,\overline{\varphi}\left[\mathfrak{B}(\beta'_j(\omega_o) - \beta'_l(\omega_o))Z_{\mathcal{A}}\right].\end{aligned} \tag{8.15}$$

The diagonal part is the same as (8.13), but the off-diagonal terms deteriorate the refocusing at the source. These terms are large when the array has small aperture $\mathcal{A}_\eta$. The best refocusing occurs for full aperture arrays, where the matrix Γ_{jl} is the identity.

8.3. Time reversal in random waveguides. If the time reversal process is statistically stable, then we can estimate the refocusing of the wave by studying the mean of (8.8). We refer to the next section for the analysis of the statistical stability.

Using the moment formula (6.28) we obtain

$$\begin{aligned}\mathbb{E}\left[\mathcal{O}(t,X^s,\eta^s)\right] \approx \frac{|\mathcal{A}_X|}{8\pi Z_{\mathcal{A}}}\sum_{j=1}^{N_T}\Gamma_{jj}\frac{\phi_j(\eta^s)\phi_j(\eta^\star)}{4\beta_j(\omega_o)} \\ \times e^{i\omega_o(T^\varepsilon-t)}\,\overline{\varphi}(B(T^\varepsilon-t))e^{i\beta_j(\omega_o)\frac{[(X^s)^2-(X^\star)^2]}{2Z_{\mathcal{A}}}} \\ \times e^{-\frac{(X^s-X^\star)^2}{2X_{d,j}^2(\omega_o)}}\operatorname{sinc}\left[\frac{\beta_j(\omega_o)(X^\star-X^s)|\mathcal{A}_X|}{2Z_{\mathcal{A}}}\right], \end{aligned} \tag{8.16}$$

where we evaluated the integrals over the bandwidth and X. The sum has only diagonal terms, so unlike in the ideal waveguide, refocusing occurs only at time $t=T^\varepsilon$, independent of the bandwidth. The time reversal function is defined by $\mathcal{J}^{\mathrm{TR}}(X^s,\eta^s)=\mathcal{O}(t=T^\varepsilon,X^s,\eta^s)$, and its mean is given by

$$\begin{aligned}\mathbb{E}\left[\mathcal{J}^{\mathrm{TR}}(X^s,\eta^s)\right] \approx \frac{|\mathcal{A}_X|\overline{\varphi}(0)}{8\pi Z_{\mathcal{A}}}\sum_{j=1}^{N_T}\Gamma_{jj}\frac{\phi_j(\eta^s)\phi_j(\eta^\star)}{\beta_j(\omega_o)}e^{i\beta_j(\omega_o)\frac{[(X^s)^2-(X^\star)^2]}{2Z_{\mathcal{A}}}} \\ \times e^{-\frac{(X^s-X^\star)^2}{2X_{d,j}^2(\omega_o)}}\operatorname{sinc}\left[\frac{\beta_j(\omega_o)(X^\star-X^s)|\mathcal{A}_X|}{2Z_{\mathcal{A}}}\right]. \end{aligned} \tag{8.17}$$

The coefficients Γ_{jj} are nonnegative,

$$\begin{aligned}\Gamma_{jj} &= \int_0^{\mathcal{D}} d\eta\, 1_{\mathcal{A}_\eta}(\eta)\phi_j^2(\eta) \\ &= \frac{|\mathcal{A}_\eta|}{\mathcal{D}} + \frac{\eta_2}{\mathcal{D}}\operatorname{sinc}\left[2\pi(j-1/2)\frac{\eta_2}{\mathcal{D}}\right] - \frac{\eta_1}{\mathcal{D}}\operatorname{sinc}\left[2\pi(j-1/2)\frac{\eta_1}{\mathcal{D}}\right] \geq 0,\end{aligned}$$

where we used the expression (2.7) of the eigenfunctions $\phi_j(\eta)$ and the aperture $\mathcal{A}_\eta=[\eta_1,\eta_2]\subset[0,\mathcal{D}]$. If the array has full aperture $\mathcal{A}_\eta=[0,\mathcal{D}]$, then $\Gamma_{jj}=1$.

8.4. Comparison of refocusing resolution in random and ideal waveguides. When we compare the expression of (8.17) with that in ideal waveguides, we see that the array aperture $\mathcal{A}_\eta$ does not play a big role in the refocusing in the random waveguide. More importantly, we show next that the refocusing is improved, which is known as superresolution.

Cross-range resolution. We observe in (8.17) that modes contribute differently to the focusing in cross-range X, with resolution

$$|X^s-X^\star| \lesssim \Delta_{X,j} := \min\left\{X_{d,j}(\omega_o), \frac{2\pi Z_{\mathcal{A}}}{\beta_j(\omega_o)|\mathcal{A}_X|}\right\}. \tag{8.18}$$

The first argument of the minimum quantifies the support of the Gaussian in (8.17) and the second argument the support of the sinc function. The latter gives the cross-range resolution in the ideal waveguide for broadband signals and arbitrary aperture $\mathcal{A}_\eta$, or for narrow-band signals and full aperture $\mathcal{A}_\eta=[0,\mathcal{D}]$.

Recall from (6.21) and (6.29) that $X_{d,j}$ decreases monotonically with j,

$$X_{d,j}(\omega_o) \approx \frac{X_{d,1}(\omega_o)}{4(j-1/2)^2} \frac{\left[(N+\alpha(\omega_o)-1/2)^2-(j-1/2)^2\right]^{1/2}}{N},$$

$$X_{d,1}(\omega_o) = \ell\sqrt{\frac{3}{2\gamma}}, \tag{8.19}$$

whereas

$$\frac{2\pi Z_{\mathcal{A}}}{\beta_j(\omega_o)|\mathcal{A}_X|} \approx \frac{2Z_{\mathcal{A}}\mathcal{D}}{|\mathcal{A}_X|}\left[(N+\alpha(\omega_o)-1/2)^2-(j-1/2)^2\right]^{-1/2} \tag{8.20}$$

increases with j. Thus, in the high-frequency regime with $N \gg 1$, the cross-range resolution for the high-order modes is determined by the decorrelation length, even for large apertures. The cross-range resolution of the first modes may be determined by the aperture, but only if it is large enough,

$$|\mathcal{A}_X| \gtrsim \frac{2Z_{\mathcal{A}}\mathcal{D}}{\ell}\sqrt{\frac{2\gamma}{3}}N. \tag{8.21}$$

In conclusion, the cross-range resolution is better in random waveguides than in ideal ones. The modes with higher indices give the best cross-range resolution, but they travel at lower speed. Thus, the focusing improves when we increase the recording time, because the array can capture the late arrivals of the high-order modes (see Figure 2). We may expect that the wave field can be sharply refocused even for small apertures $|\mathcal{A}_X|$, but we shall see in section 8.5 that large apertures increase the statistical stability (i.e., robustness) of the refocusing with respect to different realizations of the random boundary.

Depth resolution. To study the focusing in η, we evaluate (8.17) at cross-range $X^s = X^\star$. We have

$$\begin{aligned}\mathbb{E}\left[\mathcal{J}^{\mathrm{TR}}(X^\star,\eta^s)\right] &\approx \frac{|\mathcal{A}_X|\,\overline{\varphi}(0)}{8\pi Z_{\mathcal{A}}}\sum_{j=1}^{N_T}\Gamma_{jj}\frac{\phi_j(\eta^s)\phi_j(\eta^\star)}{\beta_j(\omega_o)} \\ &\approx \mathcal{J}_o^{\mathrm{TR,bb}}(X^\star,\eta^s).\end{aligned} \tag{8.22}$$

The result is the same as in ideal waveguides if the emitted signals are broadband. The time reversal function for narrowband signals in ideal waveguides is

$$\begin{aligned}\mathcal{J}_o^{\mathrm{TR,nb}}(X^\star,\eta^s) \approx \frac{|\mathcal{A}_X|}{8\pi Z_{\mathcal{A}}}\sum_{j=1}^{N}\sum_{l=1}^{N_T}\Gamma_{jl}\frac{\phi_j(\eta^s)\phi_l(\eta^\star)}{4\sqrt{\beta_j(\omega_o)\beta_l(\omega_o)}} \\ \times\, e^{i[\beta_j(\omega_o)-\beta_l(\omega_o)]\frac{Z_{\mathcal{A}}}{\varepsilon^2}}\,\overline{\varphi}\left[\mathfrak{B}(\beta_j'(\omega_o)-\beta_l'(\omega_o))Z_{\mathcal{A}}\right].\end{aligned} \tag{8.23}$$

Its diagonal ($j = l$) part is the same as (8.22), but the off-diagonal terms may have a visible effect for small apertures $\mathcal{A}_\eta$.

The sum in (8.22) is maximum at $\eta^s = \eta^\star$, because all the terms are positive. The point spread function is smaller at other depths, because of cancellations in the sum of the oscillatory terms. We can make this more explicit in the high-frequency regime, with $N \gg 1$, if we write

$$\mathcal{D} \approx \frac{\pi N}{k_o}, \qquad \phi_j(\eta) \approx \sqrt{\frac{2}{\mathcal{D}}}\cos\left[\left(j-\frac{1}{2}\right)\frac{k_o\eta}{N}\right] \tag{8.24}$$

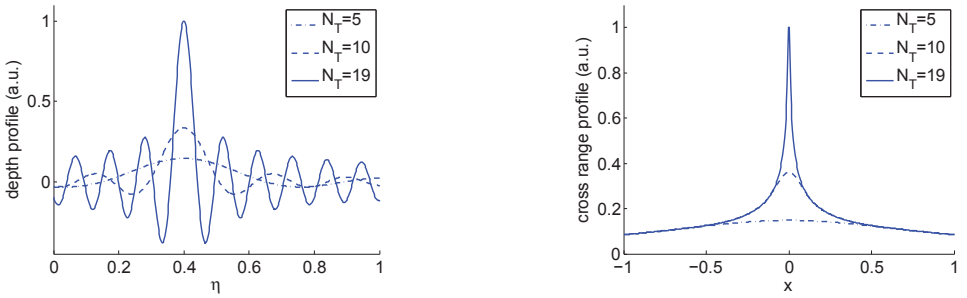

FIG. 2. *Depth profile (left) and cross-range profile (right) of the mean point spread function for the time reversal functional. Here* $Z_{\mathcal{A}} = 100$, $\ell = 1$, $\sigma = 0.25$, $k_o = 60$, $\mathcal{D} = 1$ *(so that* $N = 19$*). The array diameter* $|\mathcal{A}_X|$ *is supposed to be smaller than the critical value* (8.21)*, which is about* 220*.* N_T *is the cut-off number (modes smaller than* N_T *are recorded and reemitted). Note that the high modes play an important role. The larger* N_T *is, the better the resolution.*

and interpret (8.22) as a Riemann sum, which we then approximate with an integral. Consider for simplicity the full aperture case, where

$$\begin{aligned}\mathbb{E}\left[\mathcal{J}^{\mathrm{TR}}(X^\star,\eta^s)\right] &\approx \frac{|\mathcal{A}_X|\,\overline{\varphi}(0)}{8\pi Z_{\mathcal{A}}}\sum_{j=1}^{N_T}\frac{2}{\mathcal{D}\beta_j}\cos\left[\left(j-\frac{1}{2}\right)\frac{k_o\eta^s}{N}\right]\cos\left[\left(j-\frac{1}{2}\right)\frac{k_o\eta^\star}{N}\right]\\ &\approx \frac{|\mathcal{A}_X|}{8\pi^2 Z_{\mathcal{A}} N}\sum_{j=1}^{N_T}\frac{\cos\left[\frac{(j-1/2)}{N}k_o(\eta^\star-\eta)\right]}{\left[1-\frac{(j-1/2)^2}{N^2}\right]^{1/2}}\\ &\approx \frac{|\mathcal{A}_X|}{8\pi^2 Z_{\mathcal{A}}}\Lambda_{N_T/N}\left[k_o(\eta^s-\eta^\star)\right], \qquad \Lambda_\alpha(x)=\int_0^\alpha ds\,\frac{\cos(sx)}{\sqrt{1-s^2}}.\end{aligned} \tag{8.25}$$

The function Λ_α becomes proportional to the Bessel function of first kind J_0 as $\alpha \to 1$; more explicitly, we have $\Lambda_1(x) = (\pi/2)J_0(x)$ so that

$$\mathbb{E}\left[\mathcal{J}^{\mathrm{TR}}(X^\star,\eta^s)\right] \approx \frac{|\mathcal{A}_X|\,\overline{\varphi}(0)}{16\pi Z_{\mathcal{A}}}J_0\left[k_o(\eta^s-\eta^\star)\right] \qquad \text{if} \quad N_T \approx N. \tag{8.26}$$

We can then estimate the depth resolution as the distance between the peak of J_0, which occurs when $\eta^s = \eta^\star$, and its first zero, which occurs when $k_o|\eta^s - \eta^\star| \approx 2.4$ (first zero of J_0). Therefore, the depth resolution of time reversal with full aperture is equal to the diffraction limit

$$|\eta^s - \eta^\star| \lesssim \Delta_\eta := \frac{2.4}{k_o} \tag{8.27}$$

if the array records the waves long enough to capture almost all the propagating modes. The resolution deteriorates if N_T is much smaller than N. Indeed for small α we have $\Lambda_\alpha(x) \approx (\alpha/\pi)\,\mathrm{sinc}(\alpha x)$, and therefore the depth resolution is $\Delta_\eta \approx \pi N/(k_o N_T)$ (see Figure 2).

8.5. Statistical stability. We now show that the time reversal function is statistically stable, meaning that the refocusing of the wave at the original source location does not depend on the realization of the random medium but only on its statistical

distribution, and $\mathcal{J}^{\rm TR}$ is approximately equal to its expectation in the vicinity of the source, and in particular at $X^s = X^\star$ and $\eta^s = \eta^\star$.

We restrict the analysis of statistical stability to the case of full aperture, where the calculations are simpler because the coupling matrix Γ_{jl} becomes the identity. We obtain from (8.8) and the definition of $\mathcal{J}^{\rm TR}$ as $\mathcal{O}(t = T^\varepsilon, X^s, \eta^s)$ that

$$\mathcal{J}^{\rm TR}(X^\star, \eta^\star) \approx \sum_{j=1}^{N_T} \frac{\phi_j^2(\eta^\star)}{\beta_j^2(\omega)} \int \frac{d\omega}{2\pi B} \overline{\widehat{\varphi}}\left(\frac{\omega - \omega_o}{B}\right) \int_{-|\mathcal{A}_X|/2}^{|\mathcal{A}_X|/2} dX \ |\mathcal{T}_j(\omega, X, X^\star, Z_{\mathcal{A}})|^2 \ .$$

Let us rewrite this equation as

$$\mathcal{J}^{\rm TR}(X^s, \eta^s) = \int \frac{d\omega}{2\pi B} \overline{\widehat{\varphi}}\left(\frac{\omega - \omega_o}{B}\right) \mathcal{M}^{\rm TR}(\omega, X^\star, \eta^\star)$$

and compute first the variance of the frequency dependent kernel $\mathcal{M}^{\rm TR}$,

$$\begin{aligned} {\rm Var}\left[\mathcal{M}^{\rm TR}(\omega, X^\star, \eta^\star)\right] = \sum_{j,J=1}^{N_T} \frac{\phi_j^2(\eta^\star)}{\beta_j^2(\omega)} \frac{\phi_J^2(\eta^\star)}{\beta_J^2(\omega)} \iint_{-|\mathcal{A}_X|/2}^{|\mathcal{A}_X|/2} \\ \times dX dY \Big\{ \mathbb{E}\big[\, |\mathcal{T}_j(\omega, X, X^\star, Z_{\mathcal{A}})|^2 \, |\mathcal{T}_J(\omega, Y, X^\star, Z_{\mathcal{A}})|^2 \,\big] \\ - \mathbb{E}\big[\, |\mathcal{T}_j(\omega, X, X^\star, Z_{\mathcal{A}})|^2 \,\big] \mathbb{E}\big[\, |\mathcal{T}_J(\omega, Y, X^\star, Z_{\mathcal{A}})|^2 \,\big] \Big\}. \end{aligned}$$

From Appendix B (first case) we find that the variance is much smaller than the square expectation when $|A_X| \gg \ell$, and therefore the kernel $\mathcal{M}^{\rm TR}$ is equal to its mean approximately. The results contained in Appendix B (second case) also show that if $|A_X| < \ell$, the variance of $\mathcal{M}^{\rm TR}$ is large, and therefore that time reversal refocusing may be unstable in the narrow-band regime.

There is, however, another mechanism that can ensure statistical stability of $\mathcal{J}^{\rm TR}$ if the array is small. Indeed, if the bandwidth of the emitted signal is larger than the decorrelation frequency, then the variance

$$\begin{aligned} {\rm Var}\left[\mathcal{J}^{\rm TR}(X^\star, \eta^\star)\right] = \int \frac{d\omega}{2\pi B} \int \frac{d\omega'}{2\pi B} \overline{\widehat{\varphi}}\left(\frac{\omega - \omega_o}{B}\right) \widehat{\varphi}\left(\frac{\omega' - \omega_o}{B}\right) \\ \times {\rm Cov}\big[\mathcal{M}^{\rm TR}(\omega, X^\star, \eta^\star), \mathcal{M}^{\rm TR}(\omega', X^\star, \eta^\star)\big] \end{aligned}$$

is small because the covariance of the point spread function at two frequencies becomes approximately zero if the frequency gap is large enough. Therefore, if the pulse has large bandwidth, then the time reversal focal spot is statistically stable, even for small arrays.

9. Imaging. The improved and stable focusing of the time reversal process in the random waveguide is due the backpropagation of the time-reversed field $D^{\rm TR}$ in *exactly the same waveguide*. Time reversal is a physical experiment, where the waves can be observed in the vicinity of the source as they refocus. In imaging we have access only to the data measured at the array, and the backpropagation to the search points is synthetic. Because we cannot know the fluctuations of the boundary, we simply ignore them in the synthetic backpropagation and obtain the so-called *reversed-time migration* imaging function. We analyze it in section 9.1 and show that it does not give useful results in the low-SNR regime defined in section 6.2. In particular, we show that the images are not statistically stable with respect to

realizations of the fluctuations. Stability can be achieved by imaging with local cross-correlations of the array measurements. Local means that we recall the decorrelation properties of the random mode amplitudes described in section 6.4, and cross-correlate the measurements over receivers located at nearby cross-ranges X, and projected on the same eigenfunctions. The resulting *coherent interferometric* imaging method is analyzed in section 9.2.

9.1. Reverse-time migration. The reverse-time migration function is given by the time-reversed data $D^{\rm TR}$ propagated (migrated) in the ideal waveguide to the search points $(x^s,\eta^s,z^s)=\left(\frac{X^s}{\varepsilon},\eta^s,\frac{Z^s}{\varepsilon^2}\right)$. Its mathematical expression follows from (3.14), with amplitudes (3.12) replaced by

$$a_{j,o}(\omega,X,Z)\rightsquigarrow\int dX'\mathcal{T}_{j,o}(\omega,X,X',Z)\frac{1}{2i\beta_j(\omega)}\int_0^{\mathcal{D}}d\eta\,\phi_j(\eta)\widehat{D}^{\rm TR}(\omega,X',\eta), \tag{9.1}$$

with ideal transfer coefficients given by (8.10). We obtain

$$\begin{aligned}\mathcal{J}^{\rm M}(X^s,\eta^s,Z^s)=&\sum_{j=1}^N\phi_j(\eta^s)\int\frac{d\omega}{2\pi}\,\frac{e^{i\beta_j(\omega)\frac{Z_{\mathcal{A}}-Z^s}{\varepsilon^2}-i\omega t}}{2i\beta_j(\omega)}\int dX\int d\eta\,\phi_j(\eta)\\ &\times\widehat{D}^{\rm TR}(\omega,X,\eta)\,\mathcal{T}_{j,o}(\omega,X,X^s,Z_{\mathcal{A}}-Z^s)\Big|_{t=T^\varepsilon},\end{aligned} \tag{9.2}$$

with the right-hand side evaluated at the same time $t=T_\varepsilon$ as in time reversal.

We assume again a tightly supported source density normalized by (7.3) and substitute the model (8.4) of $\widehat{D}^{\rm TR}$ into (9.2) to obtain

$$\mathcal{J}^{\rm M}(X^s,\eta^s,Z^s)=\int\frac{d\omega}{2\pi B}\,\overline{\widehat{\varphi}}\left(\frac{\omega-\omega_o}{B}\right)\,\mathcal{M}^{\rm M}\left(\omega,X^s,\eta^s,Z^s\right), \tag{9.3}$$

with frequency-dependent kernel

$$\begin{aligned}\mathcal{M}^{\rm M}\left(\omega,X^s,\eta^s,Z^s\right)\approx&\sum_{j=1}^N\sum_{l=1}^{N_T}\Gamma_{jl}\frac{\phi_j(\eta^s)\phi_l(\eta^\star)}{4\beta_j(\omega_o)\beta_l(\omega_o)}e^{i\beta_j(\omega)\frac{Z_{\mathcal{A}}-Z^s}{\varepsilon^2}-i\beta_l(\omega)\frac{Z_{\mathcal{A}}}{\varepsilon^2}}\\ &\times\int_{-|\mathcal{A}_X|/2}^{|\mathcal{A}_X|/2}\mathcal{T}_{j,o}\Big(\omega,X,X^s,Z_{\mathcal{A}}-Z^s\Big)\overline{\mathcal{T}_l\Big(\omega,X,X^\star,Z_{\mathcal{A}}\Big)}\,.\end{aligned} \tag{9.4}$$

The derivation of this kernel is similar to that of (8.8) in section 8.1, and we recall from there that N_T is the number of modes that arrive within the recording time of the window ψ.

9.1.1. The mean imaging function. Let us take for simplicity the case of full aperture in depth, where the coupling matrix Γ_{jl} given by (8.7) becomes the identity. We obtain from (9.4), the moment formula (6.4), and the evaluation of the integral over X that

$$\begin{aligned}\mathbb{E}\left[\mathcal{M}^{\rm M}(\omega,X^s,\eta^s,Z^s)\right]\approx&\frac{|\mathcal{A}_X|}{8\pi Z_{\mathcal{A}}}\sum_{j=1}^{N_T}\frac{\phi_j(\eta^s)\phi_j(\eta^\star)}{\beta_j(\omega_o)}\\ &\times e^{-\frac{Z_{\mathcal{A}}}{S_j(\omega_o)}-i\beta_j(\omega)\frac{Z^s}{\varepsilon^2}}\mathrm{sinc}\left[\frac{\beta_j(\omega_o)|\mathcal{A}_X|}{2Z_{\mathcal{A}}}(X^s-X^\star)\right]\\ &\times e^{\frac{i\beta_j(\omega_o)}{2Z_{\mathcal{A}}}\left[(X^s)^2-(X^\star)^2\right]}.\end{aligned} \tag{9.5}$$

The result is almost the same as for time reversal in the ideal waveguide, except for the damping coefficients $\exp\left[-Z_{\mathcal{A}}/\mathcal{S}_j\right]$.

The sinc function in the mean kernel gives the focusing in cross-range, with mode-dependent resolution

$$|X^S - X^\star| \lesssim \Delta_{X,j} := \frac{2\pi Z_{\mathcal{A}}}{\beta_j(\omega_o)|\mathcal{A}_X|}. \tag{9.6}$$

The best resolution is for the first mode, which has the largest wavenumber $\beta_1(\omega_o) \approx \pi N/\mathcal{D} \approx k_o$, and gives the Rayleigh cross-range resolution

$$\Delta_{X,1} \approx \frac{2\pi Z_{\mathcal{A}}}{k_o|\mathcal{A}_X|}. \tag{9.7}$$

The focusing of the kernel $\mathcal{M}^{\mathrm{M}}$ in range can be due only to the summation of the rapidly oscillating terms $\exp\left[-i\beta_j Z^s/\varepsilon^2\right]$, at least for large enough N. But these terms are weighted by $\exp[-Z_{\mathcal{A}}/\mathcal{S}_j]$, which decay fast in j. The first term dominates in (9.5), evaluated at $X^s = X^\star$ and $\eta^s = \eta^\star$, so the mode diversity does not lead to focusing in range, as is the case in ideal waveguides. The mean reverse-time migration function peaks at $Z^s = 0$ because of the integral over the bandwidth in (9.2), and the range resolution is of the order $\varepsilon^2/[\beta_1'(\omega_o)B]$.

When we evaluate (9.5) at $Z^s = 0$ and $X^s = X^\star$, we obtain

$$\mathbb{E}\left[\mathcal{M}^{\mathrm{M}}(\omega, X^s = X^\star, \eta^s, Z^s = 0)\right] \approx \frac{|\mathcal{A}_X|}{8\pi Z_{\mathcal{A}}} \sum_{j=1}^{N_T} \frac{\phi_j(\eta^s)\phi_j(\eta^\star)}{\beta_j(\omega_o)} e^{-Z_{\mathcal{A}}/\mathcal{S}_j(\omega_o)}. \tag{9.8}$$

This is a sum of the oscillatory functions

$$\phi_j(\eta^s)\phi_j(\eta^\star) = \frac{1}{\mathcal{D}}\left\{\cos\left[\pi\left(j-\frac{1}{2}\right)\frac{(\eta^s-\eta^\star)}{\mathcal{D}}\right] + \cos\left[\pi\left(j-\frac{1}{2}\right)\frac{(\eta^s+\eta^\star)}{\mathcal{D}}\right]\right\}$$

multiplied by positive weights, which are small and decay fast in j. The first term dominates in (9.8), and there is no depth resolution at all. We show next that these small weights also indicate the lack of statistical stability of the reverse-time migration function.

9.1.2. Stability analysis. To assess the stability of the reverse-time migration, we calculate its variance at the source location

$$\mathrm{Var}\left[\mathcal{J}^{\mathrm{M}}(X^\star, \eta^\star, 0)\right] = \mathbb{E}\left[\left|\mathcal{J}^{\mathrm{M}}(X^\star, \eta^\star, 0)\right|^2\right] - \left|\mathbb{E}\left[\mathcal{J}^{\mathrm{M}}(X^\star, \eta^\star, 0)\right]\right|^2.$$

We have from the results above that

$$\mathbb{E}\left[\mathcal{J}^{\mathrm{M}}(X^\star, \eta^\star, 0)\right] \approx \frac{|\mathcal{A}_X|}{8\pi Z_{\mathcal{A}}} \int \frac{d\omega}{2\pi B}\, \overline{\widehat{\varphi}}\left(\frac{\omega-\omega_o}{B}\right) \sum_{j=1}^{N_T} \frac{\phi_j^2(\eta^\star)}{\beta_j(\omega_o)} e^{-Z_{\mathcal{A}}/\mathcal{S}_j(\omega_o)}. \tag{9.9}$$

The second moment of $\mathcal{J}^{\mathrm{M}}$ is

$$\begin{aligned}
\mathbb{E}\left[\left|\mathcal{J}^{\mathrm{M}}(X', \eta', 0)\right|^2\right] \approx & \int \frac{d\omega_1}{2\pi B} \int \frac{d\omega_2}{2\pi B}\, \overline{\widehat{\varphi}}\left(\frac{\omega_1-\omega_o}{B}\right) \widehat{\varphi}\left(\frac{\omega_2-\omega_o}{B}\right) \\
& \times \sum_{j,l=1}^{N_T} \frac{\phi_j^2(\eta^\star)\phi_l^2(\eta^\star)}{16\beta_j^2(\omega_o)\beta_l^2(\omega_o)} \iint_{-|\mathcal{A}_X|/2}^{|\mathcal{A}_X|/2} dX_1 dX_2 \\
& \times \mathcal{T}_{j,o}(\omega_1, X_1, X^\star, Z_{\mathcal{A}})\overline{\mathcal{T}_{l,o}(\omega_1, X_1, X^\star, Z_{\mathcal{A}})} \\
& \times \mathbb{E}\left[\overline{\mathcal{T}_j\left(\omega_1, X_1, X^\star, Z_{\mathcal{A}}\right)}\mathcal{T}_l\left(\omega_2, X_2, X^\star, Z_{\mathcal{A}}\right)\right],
\end{aligned}$$

and we recall from Proposition 6.3 that only the diagonal terms $j = l$ contribute to the expectation. We also assume a small bandwidth $B \ll \Omega_{d,j}$ for all the modes j, so that we can use the simpler moment formula (6.28). We obtain

$$\mathbb{E}\left[\left|\mathcal{J}^{\mathrm{M}}(X',\eta',0)\right|^2\right] \approx \frac{|\varphi(0)|^2}{(8\pi Z_{\mathcal{A}})^2}\sum_{j=1}^{N_T}\frac{\phi_j^4(\eta^\star)}{\beta_j^2(\omega_o)}\iint_{-|\mathcal{A}_X|/2}^{|\mathcal{A}_X|/2} dX_1 dX_2 e^{-\frac{(X_1-X_2)^2}{2X_{d,j}^2(\omega_o)}} \tag{9.10}$$

and, integrating in X_1 and X_2, under the assumption that the decoherence lengths $X_{d,j}$ are much smaller than the array aperture,

$$\mathbb{E}\left[\left|\mathcal{J}^{\mathrm{M}}(X',\eta',0)\right|^2\right] \approx \frac{|\varphi(0)|^2|\mathcal{A}_X|\sqrt{2\pi}}{(8\pi Z_{\mathcal{A}})^2}\sum_{j=1}^{N_T}\frac{X_{d,j}(\omega_o)\phi_j^4(\eta^\star)}{\beta_j^2(\omega_o)}. \tag{9.11}$$

The second moment (9.11) is clearly much larger than the square of the mean (9.9), which is exponentially small in range. Therefore, the variance of $\mathcal{J}^{\mathrm{M}}$ is large near the peak of its expectation. Although the mean of the imaging function is focused at the source, it cannot be observed because it is dominated by its random fluctuations. The reverse-time migration lacks statistical stability with respect to the realizations of the random fluctuations of the boundary of the waveguide.

The calculations above are for a small bandwidth, satisfying $B \ll \Omega_{d,j}$ for $j = 1,\ldots,N_T$. The calculations are more complicated for a larger bandwidth, but the conclusion remains that reverse-time migration is not stable with respect to different realizations of the random boundary fluctuations.

9.2. Coherent interferometric imaging. The main idea of the coherent interferometric (CINT) imaging approach is to backpropagate synthetically to the imaging points the local cross-correlations of the array measurements, instead of the measurements themselves. By local we mean that because of the statistical decorrelation properties of the random mode amplitudes described in section 6.4, we cross-correlate the data $\widehat{D}(\omega,X,\eta)$ at nearby frequencies and cross-ranges X, after projecting it on the subspace of one eigenfunction ϕ_j at a time. The projection gives the coefficients

$$\widehat{D}_j(\omega,X) = \int_0^{\mathcal{D}} d\eta\,\phi_j(\eta)\widehat{D}(\omega,X,\eta), \tag{9.12}$$

which are directly proportional to the coefficients $\widehat{F}_j$ of the source only in the case of an array spanning the entire depth of the waveguide. We assume this case here, because it simplifies the analysis of the focusing and stability of the CINT function. We also assume as in the previous sections a source supported tightly around the location $(X^\star,\eta^\star)$.

The model of the coefficients (9.12) is

$$\begin{aligned}\widehat{D}_j(\omega,X) \approx{}& 1_{\mathcal{A}_X}(X)\frac{\phi_j(\eta^\star)}{2i\beta_j(\omega_o)}\psi\left(\frac{\beta_j'(\omega_o)Z_{\mathcal{A}}}{T}\right)\\ &\times\frac{1}{B}\widehat{\varphi}\left(\frac{\omega-\omega_o}{B}\right)e^{i\beta_j(\omega)Z_{\mathcal{A}}/\varepsilon^2}\mathcal{T}_j\Big(\omega,X,X^\star,Z_{\mathcal{A}}\Big),\end{aligned} \tag{9.13}$$

and we cross-correlate them at cross-ranges satisfying $|X_1 - X_2| \le X_{d,j}(\omega_o)$ and at frequency offsets

$$|\omega_1 - \omega_2| \le \Omega \ll \Omega_{d,j}. \tag{9.14}$$

We take such small Ω to simplify the second moment formulas.

The CINT image is formed by backpropagating the cross-correlations to the imaging point, using the Green's function in the ideal waveguide. We first define the CINT image in the (X, Z)-domain:

$$\mathcal{J}^{\rm CINT}(X^s, Z^s) = \sum_{j=1}^{N} \mathcal{J}_j^{\rm CINT}(X^s, Z^s), \tag{9.15}$$

with

$$\begin{aligned}\mathcal{J}_j^{\rm CINT}(X^s, Z^s) = &\iint \frac{d\omega_1}{2\pi}\frac{d\omega_2}{2\pi} 1_\Omega(\omega_1-\omega_2) e^{i[\beta_j(\omega_2)-\beta_j(\omega_1)]\frac{Z^s-Z_{\mathcal{A}}}{\varepsilon^2}} \\ &\times \iint_{-|\mathcal{A}_X|/2}^{|\mathcal{A}_X|/2} dX_1 dX_2\, 1_{X_{d,j}}(X_1-X_2) \\ &\times \widehat{D}_j(\omega_1, X_1)\overline{\widehat{D}_j(\omega_2, X_2)\mathcal{T}_{j,o}\Big(\omega_1, X_1, X^s, Z_{\mathcal{A}}-Z^s\Big)} \\ &\times \mathcal{T}_{j,o}\Big(\omega_2, X_2, X^s, Z_{\mathcal{A}}-Z^s\Big),\end{aligned} \tag{9.16}$$

where $1_{X_{d,j}}$ are indicator functions of the cross-range interval $[-X_{d,j}(\omega_o), X_{d,j}(\omega_o)]$, and 1_Ω is the indicator function of the frequency interval $[-\Omega, \Omega]$.

9.2.1. The mean CINT function. To study the focusing of CINT, we consider its expectation

$$\mathbb{E}\left[\mathcal{J}^{\rm CINT}(X^s, Z^s)\right] \approx \int \frac{d\omega}{2\pi B^2} \left|\widehat{\varphi}\left(\frac{\omega-\omega_o}{B}\right)\right|^2 \mathbb{E}\left[\mathcal{M}^{\rm CINT}(\omega, X^s, Z^s)\right], \tag{9.17}$$

with frequency-dependent kernel

$$\begin{aligned}\mathbb{E}\left[\mathcal{M}^{\rm CINT}(\omega, X^s, Z^s)\right] \approx &\sum_{j=1}^{N_T} \frac{\phi_j^2(\eta^\star)}{64\pi^4 Z_{\mathcal{A}}(Z_{\mathcal{A}}-Z^s)} \int d\widetilde{\omega}\, 1_\Omega(\widetilde{\omega}) e^{i\left[\beta_j\left(\omega+\frac{\widetilde{\omega}}{2}\right)-\beta_j\left(\omega-\frac{\widetilde{\omega}}{2}\right)\right]\frac{Z^s}{\varepsilon^2}} \\ &\times \iint_{-|\mathcal{A}_X|/2}^{|\mathcal{A}_X|/2} dX_1 dX_2 e^{-\frac{(X_1-X_2)^2}{2X_{d,j}^2(\omega_o)}} e^{i\beta_j(\omega_o)\left[\frac{(X_1-X^\star)^2}{2Z_{\mathcal{A}}}-\frac{(X_1-X^s)^2}{2(Z_{\mathcal{A}}-Z^s)}-\frac{(X_2-X^\star)^2}{2Z_{\mathcal{A}}}+\frac{(X_2-X^s)^2}{2(Z_{\mathcal{A}}-Z^s)}\right]}.\end{aligned} \tag{9.18}$$

This expression follows from (9.16), the second moment formula (6.28), and definition (8.10) of the ideal transfer coefficients $\mathcal{T}_{j,o}$.

Cross-range focusing. Let us evaluate (9.18) at the range of the source $Z^s = 0$,

$$\mathbb{E}\left[\mathcal{M}^{\rm CINT}(\omega, X^s, 0)\right] \approx \frac{\Omega}{64\pi^4 Z_{\mathcal{A}}^2} \sum_{j=1}^{N^T} \phi_j^2(\eta^\star) \iint_{-|\mathcal{A}_X|/2}^{|\mathcal{A}_X|/2} e^{i\beta_j(\omega_o)\frac{(X^s-X^\star)}{Z_{\mathcal{A}}}(X_1-X_2)-\frac{(X_1-X_2)^2}{2X_{d,j}^2(\omega_o)}}. \tag{9.19}$$

This formula simplifies after integrating over the array aperture and assuming that $X_{d,j} \ll |\mathcal{A}_X|$ to

$$\mathbb{E}\left[\mathcal{M}^{\rm CINT}(\omega, X^s, 0)\right] \sim \frac{\Omega|\mathcal{A}_X|(2\pi)^{1/2}}{64\pi^4 Z_{\mathcal{A}}^2} \sum_{j=1}^{N_T} \phi_j^2(\eta^\star) X_{d,j}(\omega_o) e^{-\frac{1}{2}\left[\frac{\beta_j(\omega_o)(X^s-X^\star)X_{d,j}(\omega_o)}{Z_{\mathcal{A}}}\right]^2}. \tag{9.20}$$

Each term in the sum focuses at the source, with resolution

$$|X^s - X^\star| \lesssim \Delta_{X,j} := \frac{Z_{\mathcal{A}}}{\beta_j(\omega_o) X_{d,j}(\omega_o)} \tag{9.21}$$

defined by the standard deviation of the Gaussian in (9.20). The number of modes participating in the sum is determined by the length of the recording time window, as before, but each mode is weighted by the correlation length $X_{d,j}(\omega_o)$, which decreases monotonically with j. The first mode has the largest contribution in (9.20) and gives the best cross-range resolution. Since its wavenumber is approximately $\beta_1(\omega_o) \approx \pi N/\mathcal{D} \approx k_o$,

$$\Delta_{X,1} \approx \frac{\lambda_o Z_{\mathcal{A}}}{X_{d,1}(\omega_o)} \tag{9.22}$$

is comparable to the classic Rayleigh resolution for an array of aperture equal to $X_{d,1}(\omega_o)$ (see Figure 3).

The cross-range resolution (9.22) is worse than that of time reversal. Scattering at the random boundary is beneficial to the time reversal process, and the more modes recorded, the better the result. However, scattering impedes imaging, and the best cross-range resolution is achieved with the first mode. Even with this mode, the resolution is worse than that in ideal waveguides $2\pi Z_{\mathcal{A}}/(k_o|\mathcal{A}_X|)$, because $X_{d,1} \ll |\mathcal{A}_X|$.

Range focusing. When we evaluate the mean CINT kernel (9.18) at the cross-range $X^s = X^\star$, we obtain

$$\begin{aligned}\mathbb{E}\left[\mathcal{M}^{\mathrm{CINT}}(\omega, X^\star, Z^s)\right] \approx \sum_{j=1}^{N_T} \frac{\phi_j^2(\eta^\star)}{64\pi^4 Z_{\mathcal{A}}(Z_{\mathcal{A}} - Z^s)} \int d\widetilde{\omega}\, 1_\Omega(\widetilde{\omega}) e^{-i\left[\beta_j\left(\omega+\frac{\widetilde{\omega}}{2}\right)-\beta_j\left(\omega-\frac{\widetilde{\omega}}{2}\right)\right]\frac{Z^s}{\varepsilon^2}} \\ \times \iint_{-|\mathcal{A}_X|/2}^{|\mathcal{A}_X|/2} dX_1 dX_2\, e^{-i\beta_j(\omega_o)\frac{(X_1-X_2)Z^s}{Z_{\mathcal{A}}(Z_{\mathcal{A}}-Z^s)}\left(\frac{X_1+X_2}{2}-X^\star\right)-\frac{(X_1-X_2)^2}{2X_{d,j}^2(\omega_o)}}.\end{aligned} \tag{9.23}$$

Because we integrate over $\widetilde{\omega}$ the rapidly oscillating integrand, at scale ε^2, we have from the method of stationary phase that (9.23) is large for

$$Z^s = \varepsilon^2 \zeta^s,$$

with ζ^s independent of ε. Recall the assumption (9.14) of the frequency offsets. The mean kernel becomes

$$\mathbb{E}\left[\mathcal{M}^{\mathrm{CINT}}(\omega, X^\star, \varepsilon^2\zeta^s)\right] \approx \frac{\Omega|\mathcal{A}_X|(2\pi)^{1/2}}{64\pi^4 Z_{\mathcal{A}}^2} \sum_{j=1}^{N_T} X_{d,j}(\omega_o)\phi_j^2(\eta^\star)\mathrm{sinc}\left[\beta_j'(\omega_o)\Omega\zeta^s\right], \tag{9.24}$$

and we define the mode-dependent scaled range resolution by

$$|\zeta^s| \lesssim \Delta_{\zeta,j} := \frac{1}{\Omega\beta_j'(\omega_o)}. \tag{9.25}$$

This is similar to the classic range resolution defined as the distance traveled by the waves during the duration of the pulse. Here the propagation speed $1/\beta_j'$ is mode

dependent and, instead of the pulse, we have the time window of duration $\sim 1/\Omega$, with Fourier transform $1_\Omega(\omega)$. The first mode has the largest weight $X_{d,1}$ in (9.24), and it determines its range resolution, as illustrated in Figure 3. This is similar to what we saw above in the analysis of cross-range resolution. However, while the first mode is best for focusing in cross-range, it gives the worst range resolution, because it has the largest speed $1/\beta_1' \approx c_o$. The CINT imaging function (9.15) is not optimal for range focusing. We need weights that emphasize the contribution of the higher-order modes, which travel at speed $1/\beta_j' \ll c_o$, and give better range resolution.

Depth estimation. One natural way to estimate the depth $\eta^\star$ would be to consider the full CINT imaging function

$$\widetilde{\mathcal{J}}^{\rm CINT}(X^s,\eta^s,Z^s) = \sum_{j=1}^{N} \mathcal{J}_j^{\rm CINT}(X^s,Z^s)\phi_j^2(\eta^s),$$

with $\mathcal{J}_j^{\rm CINT}(X^s,Z^s)$ defined by (9.16). However, when we evaluate the mean of this expression at $X^s = X^\star$ and $Z^s = 0$, we obtain

$$\mathbb{E}\left[\widetilde{\mathcal{J}}^{\rm CINT}(X^\star,\eta^s,0)\right] \approx \frac{\Omega|\mathcal{A}_X|(2\pi)^{1/2}\|\mathfrak{f}\|^2}{64\pi^4 Z_{\mathcal{A}}^2} \sum_{j=1}^{N_T} X_{d,j}(\omega_o)\phi_j^2(\eta^\star)\phi_j^2(\eta^s), \tag{9.26}$$

where we used (7.5) and let $\|\mathfrak{f}\|^2$ be the mean square norm of the emitted signal. The expression (9.26) is a sum of positive terms, and it does not have a peak at the depth of the source (see Figure 4).

Because of scattering at the random boundary the modes are decoupled, and we cannot speak of coherent imaging in depth. We work instead with the squares of the mode amplitudes, i.e., intensities. Incoherent imaging means estimating the depth of the source based on the mathematical model (9.26). More explicitly, we can estimate $\eta^\star$ by solving the least squares minimization problem

$$\min_{\eta^s} \sum_{j=1}^{N_T} \left| \mathcal{J}_j^{\rm CINT}(\widehat{X}^\star,\widehat{Z}^\star) - \frac{\Omega|\mathcal{A}_X|(2\pi)^{1/2}\|\mathfrak{f}\|^2}{64\pi^4 Z_{\mathcal{A}}^2} X_{d,j}(\omega_o)\phi_j^2(\eta^s) \right|^2, \tag{9.27}$$

where the estimators $\widehat{X}^\star$ and $\widehat{Z}^\star$ of the cross-range $X^\star$ and range offset $Z^\star = 0$ of the source have been determined as the location of the maximum of (9.15) (see Figure 4).

9.2.2. Statistical stability. The analysis of statistical stability of the CINT function is basically the same as that of time reversal. The function is stable when evaluated in the vicinity of the source location if the array has large aperture $|\mathcal{A}_X| \gg \ell$. We have seen in the previous section that a large aperture does not improve the focusing of $\mathbb{E}\left[\mathcal{J}^{\rm CINT}\right]$. The cross-range resolution is limited by the decoherence length. But a large aperture is needed for the CINT function to be statistically stable.

Another way of achieving statistical stability of CINT is to have a pulse with large bandwidth. This was already noted in the discussion of statistical stability of time reversal in section 8.5.

Note that the statistical stability of CINT relies on computing correctly the local cross-correlations of the measurements at the array. By this we mean that the cross-range and frequency offsets in the correlations should not exceed the decoherence length and frequency. Moreover, the cross-correlations should be with one mode at a time. This can be done with arrays that span the whole depth of the waveguide,

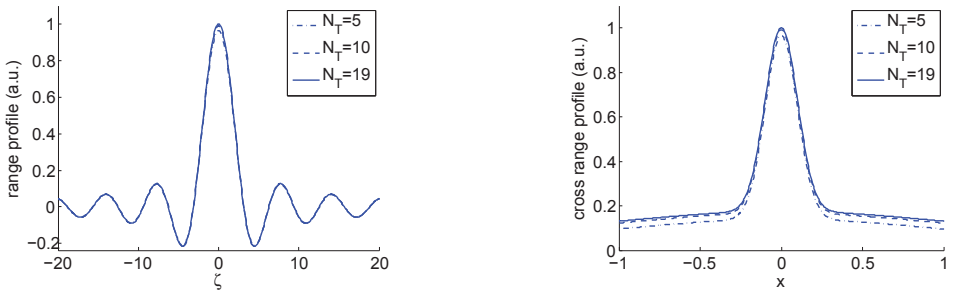

FIG. 3. *Range profile and cross-range profile of the mean point spread function for the CINT functional. Here* $Z_{\mathcal{A}} = 100$, $\ell = 1$, $\sigma = 0.25$, $k_o = 60$, $\mathcal{D} = 1$ *(so that* $N = 19$*), and the cut-off frequency is* $\Omega/c = 1$. N_T *is the cut-off number (modes smaller than* N_T *are recorded and reemitted). Note that the high modes do not play any role.*

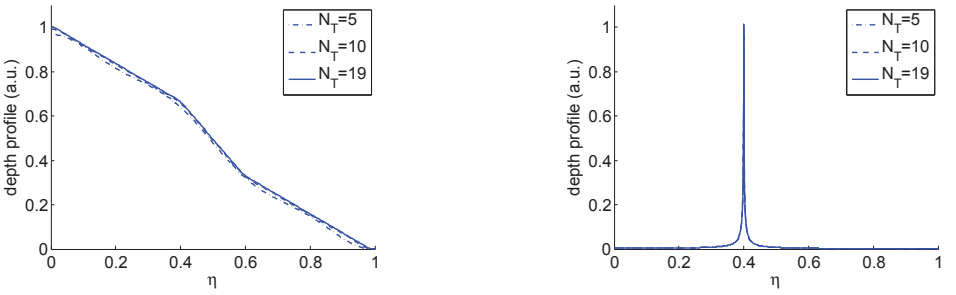

FIG. 4. *Depth profile with* (9.26) *(left) and with* (9.27) *(right) for the CINT functional. In the right picture we plot the reciprocal of the square root of the function in* (9.27). *Here* $Z_{\mathcal{A}} = 100$, $\ell = 1$, $\sigma = 0.25$, $k_o = 60$, $\mathcal{D} = 1$ *(so that* $N = 19$*). N_T is the cut-off number (modes smaller than N_T are recorded and reemitted). Note that the high modes do not play any role.*

because the coupling matrix Γ_{jl} becomes the identity when $|\mathcal{A}_\eta| = \mathcal{D}$. If the aperture $|\mathcal{A}_\eta|$ is small, there are large mode index offsets $|j-l|$ for which $\Gamma_{jl} \neq 0$. Consequently, there are many terms of the form $\overline{\mathcal{T}_j}\mathcal{T}_l$, with $j \neq l$, that participate in the expression of the imaging function. Since only the diagonal terms are correlated, we obtain that $\mathcal{J}^{\text{CINT}}$ has large variance when $|\mathcal{A}_\eta| \ll \mathcal{D}$.

In practice, the decoherence scales $X_{d,j}$ and $\Omega_{d,j}$ are likely not known explicitly. The formulas derived above are specific to our mathematical model. However, the decoherence scales can be estimated as we form the image, using an adaptive procedure similar to that introduced in [5].

10. Summary. In this paper we analyze propagation of acoustic waves in three-dimensional random waveguides. The waves are trapped by top and bottom boundaries, but the medium is unbounded in the remaining two directions. The top boundary has small, random fluctuations. We consider a source that emits a beam and study the resulting random wave field in the waveguide.

The analysis is in a long range, paraxial scaling regime modeled with a small parameter ε. It is defined as the ratio of the central wavelength λ_0 of the pulse emitted from the source and the emitted beam width r_0. The range of propagation is of the order of the Rayleigh length $r_0^2/\lambda_0 = \varepsilon^{-2}\lambda_0$. The fluctuations of the boundary are on a length scale that is similar to the beam width, and their small amplitude

is scaled so that they cause significant cumulative scattering effects when the waves travel at ranges of the order of the Rayleigh length.

The wave field is given by a superposition of waveguide modes with random amplitudes. The mode profiles are solutions of the wave equation in the ideal waveguide, with flat boundary. The scattering effects are captured by their random amplitudes. We show that in our scaling regime the mode amplitudes satisfy a system of paraxial equations driven by the same Brownian field. We use the system to calculate three important mode-dependent scales that quantify the net scattering effects in the waveguide and play a key role in applications such as imaging and time reversal. The first mode-dependent scale is the scattering mean free path. It gives the range over which the mode loses its coherence, meaning that the expectation of its random amplitude is smaller than the standard deviation of its fluctuations. The other mode-dependent scales are the decoherence length and frequency. They give the cross-range scale and frequency offsets over which the mode amplitudes become statistically uncorrelated.

We use the results of the analysis to study time reversal and imaging of the source with a remote array of sensors in a low-SNR regime. Low SNR means that the waves travel over distances that exceed the scattering mean free paths of all the modes, so that the random wave field measured at the array is dominated by its fluctuations.

In time reversal, the waves received at the array are time-reversed and then reemitted in the medium. They travel back to the source and refocus. The refocusing is expected by the time reversibility of the wave equation, but the resolution is limited in ideal waveguides by the aperture of the array. We analyze the time reversal process in the random waveguide and show that superresolution occurs, meaning that scattering at the random boundary improves the refocusing resolution. An essential part of the resolution analysis is the assessment of statistical stability with respect to different realizations of the random boundary fluctuations. We show that statistical stability holds if the array has large aperture and/or the emitted pulse from the source has a large bandwidth.

Time reversal is very different from imaging. In time reversal the array measurements are backpropagated physically, in the real waveguide. In imaging we can only backpropagate the time-reversed data in software, in a surrogate waveguide. Because we cannot know the boundary fluctuations, we neglect them altogether, and the surrogate is the ideal waveguide. The resulting imaging function is called reverse-time migration, and it does not work in low-SNR regimes. It lacks statistical stability; i.e., the images change unpredictably from one realization of the fluctuations of the random boundary to another.

We show that robust imaging can be carried out in low-SNR regimes if we backpropagate local cross-correlations of the array measurements, instead of the measurements themselves. Here local means that we cross-correlate the data projected on one mode at a time, and for nearby cross-ranges and frequencies. The method is called coherent interferometric (CINT), because it is an extension of the CINT approach introduced and analyzed in [7, 5, 6, 4] for imaging in open, random environments. We show that CINT images are statistically stable under two conditions: The first condition is the same as in time reversal, and it says that the array should have a large aperture and/or the pulse bandwidth should be large. The second condition is that the cross-range and frequency offsets used in the calculation of the local cross-correlations do not exceed the mode-dependent decoherence length and frequency, respectively. We derived mathematical expressions of these scales for our model. In practice, they can be estimated adaptively, using the image formation, with an ap-

proach similar to that in [5]. The estimation is possible because there is a trade-off between stability and resolution that is quantified by the decoherence scales. If we overestimate them, we lose statistical stability. If we underestimate them, we lose resolution.

While cumulative scattering aids in time reversal, it impedes imaging. We quantify this explicitly in the resolution analysis of CINT. In time reversal the resolution improves when we record the wave field over a long time, so that we include the high-order modes that travel at a slower speed. In CINT, the best cross-range and range resolution is given by the first mode, which encounters the random boundary less often and is thus less affected by the fluctuations. The cross-range resolution is similar to the classic Rayleigh one of range times wavelength divided by the aperture, but instead of the real aperture we have the decoherence length of the mode. This length decreases monotonically with range, because longer distances of propagation in the random waveguide mean stronger scattering effects. Similarly, the range resolution is similar to the classic one, of speed divided by the bandwidth, but the bandwidth is replaced by the decoherence frequency which decreases monotonically with range.

The estimation of the depth of the source is different from that of range and cross-range. Because the modes decorrelate in the low-SNR regime, we cross-correlate the data projected on one mode at a time, so essentially we work with intensities. The estimation of the depth of the source from the intensities can be done by minimizing the misfit between the processed measurements and the mathematical model. While the cross-range and range estimation with CINT is done best with the first waveguide mode, the depth estimation requires many modes. Thus, we still need a long recording time at the array to capture the later arrival of the high-order modes.

Appendix A. Second moment calculation. The following equation is for $\mathbb{E}\left[\mathcal{T}_j(\omega_1, X_1, X_1', Z)\overline{\mathcal{T}_l}(\omega_2, X_2, X_2', Z)\right]$, which results from (5.21), using Itô calculus:

(A.1)
$$\begin{aligned}&\partial_Z \mathbb{E}\left[\mathcal{T}_j\overline{\mathcal{T}_l}\right]\\ &= \left[\frac{i}{2\beta_j(\omega_1)}\partial_{X_1}^2 - \frac{i}{2\beta_l(\omega_2)}\partial_{X_2}^2 - \left(\frac{1}{\sqrt{\mathcal{S}_j(\omega_1)}} - \frac{1}{\sqrt{\mathcal{S}_l(\omega_2)}}\right)^2 \frac{2C_o(X_1 - X_2)}{\sqrt{\mathcal{S}_j(\omega_1)\mathcal{S}_l(\omega_2)}}\right]\\ &\quad \times \mathbb{E}\left[\mathcal{T}_j\overline{\mathcal{T}_l}\right].\end{aligned}$$

Its solution can be written as

$$\begin{aligned}&\mathbb{E}\left[\mathcal{T}_j(\omega_1, X_1, X_1', Z)\overline{\mathcal{T}_l(\omega_2, X_2, X_2', Z)}\right]\\ &= M_{jl}(\omega_1, \omega_2, X_1, X_2, Z; X_1', X_2')e^{-\left(\frac{1}{\sqrt{\mathcal{S}_j(\omega_1)}} - \frac{1}{\sqrt{\mathcal{S}_l(\omega_2)}}\right)^2 Z},\end{aligned} \tag{A.2}$$

with M_{jl} solving

$$\partial_Z M_{jl} = \left[\frac{i}{2\beta_j(\omega_1)}\partial_{X_1}^2 - \frac{i}{2\beta_l(\omega_2)}\partial_{X_2}^2 - \frac{2C_o(X_1 - X_2)}{\sqrt{\mathcal{S}_j(\omega_1)\mathcal{S}_l(\omega_2)}}\right] M_{jl} \tag{A.3}$$

for $Z > 0$ and the initial condition

$$M_{jl}(\omega_1, \omega_2, X_1, X_2, 0; X_1', X_2') = \delta(X_1 - X_1')\delta(X_2 - X_2'). \tag{A.4}$$

A.1. Single frequency. Let us begin with the single frequency case, $\omega_1 = \omega_2 = \omega$, and introduce the center and difference coordinates ξ and $\widetilde{\xi}$ so that

$$X_1 = \frac{\xi + \widetilde{\xi}/2}{\sqrt{\beta_j(\omega)}}, \quad X_2 = \frac{\xi - \widetilde{\xi}/2}{\sqrt{\beta_l(\omega)}}. \tag{A.5}$$

In this coordinate system we have that

$$U_{jl}(\omega, \xi, \widetilde{\xi}, Z; \xi', \widetilde{\xi}') = M_{jl}\left(\omega, \omega, \frac{\xi + \widetilde{\xi}/2}{\sqrt{\beta_j(\omega)}}, \frac{\xi - \widetilde{\xi}/2}{\sqrt{\beta_l(\omega)}}, Z; \frac{\xi' + \widetilde{\xi}'/2}{\sqrt{\beta_j(\omega)}}, \frac{\xi' - \widetilde{\xi}'/2}{\sqrt{\beta_l(\omega)}}\right) \tag{A.6}$$

satisfies the initial value problem

(A.7)

$$\partial_Z U_{jl} = i\partial_\xi \partial_{\widetilde{\xi}} U_{jl} - \frac{2}{\sqrt{\mathcal{S}_j \mathcal{S}_l}} C_o \left[\left(\frac{1}{\sqrt{\beta_j}} - \frac{1}{\sqrt{\beta_l}}\right)\xi + \left(\frac{1}{\sqrt{\beta_j}} + \frac{1}{\sqrt{\beta_l}}\right)\frac{\widetilde{\xi}}{2}\right] U_{jl}, \qquad Z > 0,$$
$$U_{jl} = \sqrt{\beta_j \beta_l}\, \delta(\xi - \xi')\delta(\widetilde{\xi} - \widetilde{\xi}'), \qquad Z = 0.$$

Its Fourier transform in $\widetilde{\xi}$ is the Wigner distribution

$$W_{jl}(\omega, \xi, \widetilde{\kappa}, Z; \xi', \widetilde{\xi}') = \int_{-\infty}^{\infty} \frac{d\widetilde{\xi}}{2\pi} U_{jl}(\omega, \xi, \widetilde{\xi}, Z; \xi', \widetilde{\xi}') e^{-i\widetilde{\kappa}\widetilde{\xi}}, \tag{A.8}$$

the solution of the transport equation

$$[\partial_Z + \widetilde{\kappa}\partial_\xi]\, W_{jl}(\omega, \xi, \widetilde{\kappa}, Z; \xi', \widetilde{\xi}') = -\frac{4\sqrt{\beta_l}}{\sqrt{\mathcal{S}_j \mathcal{S}_l}(\sqrt{\beta_j} + \sqrt{\beta_l})} \int dq\, \widehat{C}_o\left(q \frac{2\sqrt{\beta_l}}{(\sqrt{\beta_j} + \sqrt{\beta_l})}\right)$$
$$\times \exp\left[-\frac{iq\xi}{\sqrt{\beta_j}} \frac{2(\sqrt{\beta_j} - \sqrt{\beta_l})}{(\sqrt{\beta_j} + \sqrt{\beta_l})}\right] W_{jl}\left(\omega, \xi, \widetilde{\kappa} - \frac{q}{\sqrt{\beta_j}}, Z; \xi', \widetilde{\xi}'\right) \tag{A.9}$$

for $Z > 0$, with initial condition

$$W_{jl}(\omega, \xi, \widetilde{\kappa}, 0; \xi', \widetilde{\xi}') = \frac{\sqrt{\beta_j \beta_l}}{2\pi} e^{-i\widetilde{\kappa}\widetilde{\xi}'} \delta(\xi - \xi') \tag{A.10}$$

and kernel

$$\widehat{C}_o(\kappa) = \delta(\kappa) - \frac{\widehat{R}_o(\kappa)}{R_o(0)}. \tag{A.11}$$

Here

$$\widehat{R}_o(\kappa) = \frac{1}{2\pi} \int R_o(\xi) e^{-i\kappa\cdot\xi} d\xi.$$

A.1.1. Single mode moments. The transport equation (A.9) simplifies in the case $j = l$,

$$[\partial_Z + \widetilde{\kappa}\partial_\xi]\, W_{jj}(\omega, \xi, \widetilde{\kappa}, Z; \xi', \widetilde{\xi}') = -\frac{2}{\mathcal{S}_j} \int dq\, \widehat{C}_o(q) W_{jl}\left(\omega, \xi, \widetilde{\kappa} - \frac{q}{\sqrt{\beta_j}}, Z; \xi', \widetilde{\xi}'\right),$$
$$W_{jj}(\omega, \xi, \widetilde{\kappa}, 0; \xi', \widetilde{\xi}') = \frac{\beta_j}{2\pi} e^{-i\widetilde{\kappa}\widetilde{\xi}'} \delta(\xi - \xi'), \tag{A.12}$$

and can be integrated easily after Fourier transforming in $\widetilde{\kappa}$ and ξ. Explicitly,

$$V_{jj}(\omega,\kappa,\widetilde{\xi},Z;\xi',\widetilde{\xi}') = \int_{-\infty}^{\infty}\frac{d\xi}{2\pi}\int_{-\infty}^{\infty} d\widetilde{\kappa}\, W_{jj}(\omega,\xi,\widetilde{\kappa},Z;\xi',\widetilde{\xi}')e^{-i\kappa\xi+i\widetilde{\kappa}\widetilde{\xi}} \tag{A.13}$$

satisfies the initial value problem

$$\left[\partial_Z+\kappa\partial_{\widetilde{\xi}}\right]V_{jj}(\omega,\kappa,\widetilde{\xi},Z;\xi',\widetilde{\xi}') = -\frac{2}{\mathcal{S}_j}C_o\left(\frac{\widetilde{\xi}}{\sqrt{\beta_j}}\right)V_{jj}(\omega,\kappa,\widetilde{\xi},Z;\xi',\widetilde{\xi}'), \qquad Z>0,$$

$$V_{jj}(\omega,\kappa,\widetilde{\xi},0;\xi',\widetilde{\xi}') = \frac{\beta_j}{2\pi}e^{-i\kappa\xi'}\delta(\widetilde{\xi}-\widetilde{\xi}'), \tag{A.14}$$

which can be solved with the method of characteristics.

We obtain that

$$V_{jj}(\omega,\kappa,\widetilde{\xi},Z;\xi',\widetilde{\xi}') = \frac{\beta_j}{2\pi}e^{-i\kappa\xi'}\,\delta\left(\widetilde{\xi}-\widetilde{\xi}'-\kappa Z\right)\exp\left[-\frac{2}{\mathcal{S}_j}\int_0^Z ds\, C_o\left(\frac{\widetilde{\xi}'+\kappa s}{\sqrt{\beta_j}}\right)\right], \tag{A.15}$$

and tracing back out transformations (A.2), (A.6), (A.8), and (A.13), we get

$$\mathbb{E}\left[\mathcal{T}_j(\omega,X_1,X_1',Z)\overline{\mathcal{T}_j(\omega,X_2,X_2',Z)}\right] = \frac{\beta_j}{2\pi Z}\exp\left[\frac{i\beta_j[(X_1-X_1')^2-(X_2-X_2')^2]}{2Z}\right.$$
$$\left. -\frac{2}{\mathcal{S}_j}\int_0^Z ds\, C_o\Big[(X_1-X_2)\frac{s}{Z}+(X_1'-X_2')\left(1-\frac{s}{Z}\right)\Big]\right]. \tag{A.16}$$

This is the result stated in Proposition 6.1.

A.1.2. Two mode moments. It is not possible to obtain a closed form solution of (A.9), unless we make further assumptions. We consider the low-SNR regime described in section 6.2 and suppose that

$$|X_1-X_2| \lesssim X_{d,j}(\omega) \ll \ell. \tag{A.17}$$

This is the condition under which the diagonal moments $\mathbb{E}\left[\mathcal{T}_j\overline{\mathcal{T}_j}\right]$ are not exponentially small, by Proposition 6.2. The two mode moments cannot be larger than the diagonal ones, so they are essentially zero when (A.17) does not hold.

Note that in (A.9) $\widetilde{\kappa}$ is the dual variable to $\widetilde{\xi}\sim\sqrt{\beta_j}(X_1-X_2)$, and that q is in the support of $\widehat{C}_o$, so $|q|\le 1/\ell$. Therefore,

$$|\widetilde{\kappa}| \sim \frac{1}{\sqrt{\beta_j}|X_1-X_2|} \gg \frac{1}{\sqrt{\beta_j}\ell} \gtrsim \frac{|q|}{\sqrt{\beta_j}},$$

and we can expand the Wigner transform in (A.9) around $\widetilde{\kappa}$. The exponential can also be expanded when

$$\frac{q\xi}{\sqrt{\beta_j}}\frac{2|\sqrt{\beta_j}-\sqrt{\beta_l}|}{(\sqrt{\beta_j}+\sqrt{\beta_l})} \lesssim \frac{X}{\ell}\frac{2|\sqrt{\beta_j}-\sqrt{\beta_l}|}{(\sqrt{\beta_j}+\sqrt{\beta_l})} \ll 1, \tag{A.18}$$

meaning that j and l are close. We return at the end of this section to this point.

Assumptions (A.17)–(A.18) justify the approximation of the right-hand side in (A.9) by the second-order expansion in q of the product of the exponential and the Wigner transform. We obtain that

(A.19)
$$(\partial_Z + \widetilde{\kappa}\partial_\xi)\, W_{jl} \approx -\frac{1}{\beta_j \ell^2 \sqrt{\mathcal{S}_j \mathcal{S}_l}} \left(\frac{\sqrt{\beta_j} + \sqrt{\beta_l}}{2\sqrt{\beta_l}} \right)^2 \left[i\partial_{\widetilde{\kappa}} - \xi \frac{2(\sqrt{\beta_j} - \sqrt{\beta_l})}{(\sqrt{\beta_j} + \sqrt{\beta_l})} \right]^2 W_{jl}$$

for $Z > 0$, with initial condition (A.10). This equation is solved in [9]. The result follows from the inverse Fourier transform in $\widetilde{\kappa}$ of the solution, and from (A.2), (A.6),

(A.20)
$$\begin{aligned}
\mathbb{E}\left[\mathcal{T}_j(\omega, X_1, X_1', Z)\overline{\mathcal{T}_l(\omega, X_2, X_2', Z)}\right] \approx \frac{\sqrt{\beta_j\beta_l}}{2\pi Z} \mathrm{sinc}^{-\frac{1}{2}} \left\{ \frac{(1+i)Z}{\ell} \left[\frac{\beta_j - \beta_l}{\beta_j\beta_l\sqrt{\mathcal{S}_j\mathcal{S}_l}} \right]^{\frac{1}{2}} \right\} \\
\times \exp\left\{ -\left(\frac{1}{\sqrt{\mathcal{S}_j}} - \frac{1}{\sqrt{\mathcal{S}_l}} \right)^2 Z + \frac{i|(X_1 - X_1')\beta_j - (X_2 - X_2')\beta_l|^2}{2Z(\beta_j - \beta_l)} \right. \\
+ \frac{\beta_j\beta_l\left(|X_1 - X_2|^2 + |X_1' - X_2'|^2\right)}{\ell(\beta_j - \beta_l)(1+i)} \left[\frac{\beta_j - \beta_l}{\beta_j\beta_l\sqrt{\mathcal{S}_j\mathcal{S}_l}} \right]^{\frac{1}{2}} \cot\left[\frac{(1+i)Z}{\ell} \left[\frac{\beta_j - \beta_l}{\beta_j\beta_l\sqrt{\mathcal{S}_j\mathcal{S}_l}} \right]^{\frac{1}{2}} \right] \\
\left. - \frac{2\beta_j\beta_l(X_1 - X_2)(X_1' - X_2')}{\ell(\beta_j - \beta_l)(1+i)} \left[\frac{\beta_j - \beta_l}{\beta_j\beta_l\sqrt{\mathcal{S}_j\mathcal{S}_l}} \right]^{\frac{1}{2}} \sin^{-1}\left[\frac{(1+i)Z}{\ell} \left[\frac{\beta_j - \beta_l}{\beta_j\beta_l\sqrt{\mathcal{S}_j\mathcal{S}_l}} \right]^{\frac{1}{2}} \right] \right\}.
\end{aligned}$$

Formula (A.20) is complicated, but it can be simplified under the assumption that

(A.21)
$$\frac{Z^2|\beta_j - \beta_l|}{\beta_j\beta_l\ell^2\sqrt{\mathcal{S}_j\mathcal{S}_l}} \ll 1.$$

Then, we can expand the sinc, cot, and $\sin^{-1}$ functions in (A.20) and obtain the simpler formula

(A.22)
$$\begin{aligned}
&\mathbb{E}\left[\mathcal{T}_j(\omega, X_1, X_1', Z)\overline{\mathcal{T}_l(\omega, X_2, X_2', Z)}\right] \approx \frac{\sqrt{\beta_j\beta_l}}{2\pi Z} \\
&\times \exp\left[\frac{i(\beta_j(X_1 - X_1')^2 - \beta_l(X_2 - X_2')^2)}{2Z} \right] \\
&\times \exp\left[-\left(\frac{1}{\sqrt{\mathcal{S}_j}} - \frac{1}{\sqrt{\mathcal{S}_l}} \right)^2 Z - \frac{(X_1 - X_2)^2 + (X_1' - X_2')^2 + (X_1 - X_2)(X_1' - X_2')}{2\sqrt{X_{d,j}X_{d,l}}} \right].
\end{aligned}$$

It remains to justify assumptions (A.18) and (A.21). Because of the exponential decay in Z, we note that the moments are essentially zero unless

$$\left(\frac{1}{\sqrt{\mathcal{S}_j}} - \frac{1}{\sqrt{\mathcal{S}_l}} \right)^2 Z \lesssim 1.$$

But in our low-SNR regime this translates to

$$\left(1 - \sqrt{\frac{\mathcal{S}_j}{\mathcal{S}_l}} \right)^2 \lesssim \frac{\mathcal{S}_j}{\gamma\mathcal{S}_1} \ll 1,$$

by definition (6.11), and it is satisfied only when $j = l$. This justifies the assumptions, and it means that the modes are essentially decorrelated.

A.2. Two frequency moments. The calculation of the two frequency moments is exactly as in the previous section, with β_j replaced by $\beta_j(\omega_1)$ and β_l replaced by $\beta_j(\omega_2)$. We consider only the case $j = l$, because the modes decorrelate as explained above. The moment formula follows from (A.20), with β_j replaced by $\beta_j(\omega_1)$ and β_l replaced by $\beta_j(\omega_2)$, and similarly for $\mathcal{S}_j$ and $\mathcal{S}_l$. We can simplify it under the assumption that $|\omega_1-\omega_2|$ is sufficiently small to make first-order expansions in $\omega_1-\omega_2$. Let $\widetilde{\omega}$ and ω be the center and difference frequencies

$$\widetilde{\omega} = \omega_1 - \omega_2, \qquad \omega = \frac{\omega_1 + \omega_2}{2}.$$

We have from (A.20) that

$$\begin{aligned}
\mathbb{E}\left[\mathcal{T}_j\left(\omega+\frac{\widetilde{\omega}}{2},X_1,X_1',Z\right)\overline{\mathcal{T}_l\left(\omega-\frac{\widetilde{\omega}}{2},X_2,X_2',Z\right)}\right] &\approx \frac{\beta_j(\omega)}{2\pi Z}\mathrm{sinc}^{-\frac{1}{2}}\left\{\frac{(1+i)Z}{\ell\beta_j(\omega)}\left[\frac{\widetilde{\omega}\partial_\omega\beta_j(\omega)}{\mathcal{S}_j(\omega)}\right]^{\frac{1}{2}}\right\}\\
\times\exp\left\{-\widetilde{\omega}^2\Big(\partial_\omega\frac{1}{\sqrt{\mathcal{S}_j(\omega)}}\Big)^2 Z + + \frac{i|[(X_1-X_1')-(X_2-X_2')]\beta_j(\omega)+\widetilde{\omega}\frac{[(X_1-X_1')+(X_2-X_2')]}{2}\beta_j'(\omega)|^2}{2Z\widetilde{\omega}\beta_j'(\omega)}\right.\\
+\frac{\beta_j(\omega)[|X_1-X_2|^2+|X_1'-X_2'|^2]}{\ell\widetilde{\omega}\beta_j'(\omega)(1+i)}\left[\frac{\widetilde{\omega}\beta_j'(\omega)}{\mathcal{S}_j(\omega)}\right]^{\frac{1}{2}}\cot\left[\frac{(1+i)Z}{\beta_j(\omega)\ell}\left[\frac{\widetilde{\omega}\beta_j'(\omega)}{\mathcal{S}_j(\omega)}\right]^{\frac{1}{2}}\right]\\
\left.-\frac{2\beta_j(\omega)(X_1-X_2)(X_1'-X_2')}{\ell\widetilde{\omega}\beta_j'(\omega)(1+i)}\left[\frac{\widetilde{\omega}\beta_j'(\omega)}{\mathcal{S}_j(\omega)}\right]^{\frac{1}{2}}\sin^{-1}\left[\frac{(1+i)Z}{\beta_j(\omega)\ell}\left[\frac{\widetilde{\omega}\beta_j'(\omega)}{\mathcal{S}_j(\omega)}\right]^{\frac{1}{2}}\right]\right\}. \qquad \text{(A.23)}
\end{aligned}$$

A.3. Frequency decorrelation. To study the decorrelation over frequency offsets, let $X_1 = X_2$ and $X_1' = X_2'$ in (A.23):

$$\begin{aligned}
&\mathbb{E}\left[\mathcal{T}_j\Big(\omega+\frac{\widetilde{\omega}}{2},X,X',Z\Big)\overline{\mathcal{T}_j\Big(\omega-\frac{\widetilde{\omega}}{2},X,X',Z\Big)}\right]\\
&\approx\frac{\beta_j(\omega)}{2\pi Z}\mathrm{sinc}^{-\frac{1}{2}}\left\{\frac{(1+i)Z}{\ell\beta_j(\omega)}\left[\frac{\widetilde{\omega}\partial_\omega\beta_j(\omega)}{\mathcal{S}_j(\omega)}\right]^{\frac{1}{2}}\right\}\\
&\times\exp\left\{-\Big[\widetilde{\omega}\partial_\omega\mathcal{S}_j^{-\frac{1}{2}}(\omega)\Big]^2 Z+\frac{i\widetilde{\omega}\beta_j'(\omega)(X-X')^2}{2Z}\right\}. \qquad \text{(A.24)}
\end{aligned}$$

We have two factors that decay exponentially in $\widetilde{\omega}$. The first is the sinc, decaying at the rate

$$|\widetilde{\omega}| \ll \Omega_{d,j}(\omega) = \frac{\mathcal{S}_j(\omega)\beta_j^2(\omega)\ell^2}{Z^2|\beta_j'(\omega)|} = \frac{\beta_j(\omega)}{|\beta_j'(\omega)|}\frac{\mathcal{S}_j(\omega)\beta_j(\omega)\ell^2}{\gamma^2\mathcal{S}_1^2(\omega)}, \qquad \text{(A.25)}$$

and the second is the Gaussian with standard deviation

$$\Omega_j(\omega) = \frac{1}{\sqrt{2Z}\left|\partial_\omega\mathcal{S}_j^{-\frac{1}{2}}(\omega)\right|} = \frac{\beta_j(\omega)}{|\beta_j'(\omega)|}\sqrt{\frac{\mathcal{S}_j(\omega)}{2\gamma\mathcal{S}_1(\omega)}}. \qquad \text{(A.26)}$$

Note that

$$\frac{|\beta_j'(\omega)|}{\beta_j(\omega)} = \frac{(N+\alpha(\omega)-1/2)^2}{\omega\left[(N+\alpha(\omega)-1/2)^2-(j-1/2)^2\right]}, \qquad \text{(A.27)}$$

and using (2.13), (2.14), (6.3), and the high-frequency assumption $N \gg 1$, we have

$$\Omega_{d,j}(\omega) \approx \frac{\omega \ell^2 \beta_1(\omega)}{16\gamma^2 \mathcal{S}_1(\omega)} \frac{\left[\left(N+\alpha(\omega)-\frac{1}{2}\right)^2 - \left(j-\frac{1}{2}\right)^2\right]^{5/2}}{N^5 (j-1/2)^4}. \tag{A.28}$$

Here

$$\frac{\ell^2 \beta_1}{\mathcal{S}_1(\omega)} \approx \frac{\sigma^2}{32N}\left(\frac{\pi \ell}{\mathcal{D}}\right)^3 \approx \frac{\sigma^2 (\ell k)^3}{32N^4} = \frac{\pi^3 \sigma^2 (\ell/\lambda)^3}{4N^4}, \tag{A.29}$$

and $\ell/\lambda = O(1)$, because the scaled correlation length is similar to the wavelength λ. Moreover, the rate (A.26) is given by

$$\Omega_j(\omega) \approx \frac{\omega}{4\sqrt{2\gamma}} \frac{\left[\left(N+\alpha(\omega)-\frac{1}{2}\right)^2 - \left(j-\frac{1}{2}\right)^2\right]^{3/2}}{N^3 (j-1/2)^2}, \tag{A.30}$$

and it is larger than $\Omega_{d,j}(\omega)$.

Thus, we call $\Omega_{d,j}(\omega)$ the mode-dependent *decoherence frequency*, the frequency scale over which the second moments decay. Note that when the frequency offsets satisfy $|\widetilde{\omega}| \ll \Omega_{d,j}$ the moment formula (A.24) simplifies to expression (6.28) in Proposition 6.3, because

$$\exp\left[-\frac{\widetilde{\omega}^2}{2\Omega_j^2(\omega)}\right] \approx 1,$$

when

$$|\widetilde{\omega}| \ll \Omega_{d,j} \ll \Omega_j(\omega).$$

Appendix B. The fourth moments. We denote the moments by

$$M_{jlJL} := \mathbb{E}\left[\mathcal{T}_j(\omega_1, X_1, X_1', Z)\overline{\mathcal{T}_l(\omega_2, X_2, X_2', Z)}\mathcal{T}_J(\omega_3, Y_1, Y_1', Z)\overline{\mathcal{T}_L(\omega_4, Y_2, Y_2', Z)}\right] \tag{B.1}$$

and obtain from (5.21) that they satisfy the partial differential equation

$$\begin{aligned}
\partial_Z M_{jlJL} \;=\; & \left[\frac{i}{2\beta_j}\partial_{X_1}^2 - \frac{i}{2\beta_l}\partial_{X_2}^2 + \frac{i}{2\beta_J}\partial_{Y_1}^2 - \frac{i}{2\beta_L}\partial_{Y_2}^2\right] M_{jlJL} \\
& + \left[-\left(\frac{1}{\sqrt{\mathcal{S}_j}} - \frac{1}{\sqrt{\mathcal{S}_l}}\right)^2 - \left(\frac{1}{\sqrt{\mathcal{S}_J}} - \frac{1}{\sqrt{\mathcal{S}_L}}\right)^2 - \frac{2C_o(X_1-X_2)}{\sqrt{\mathcal{S}_j\mathcal{S}_l}} - \frac{2C_o(Y_1-Y_2)}{\sqrt{\mathcal{S}_J\mathcal{S}_L}}\right] M_{jlJL} \\
& + \frac{2}{R_o(0)}\left[\frac{R_o(X_1-Y_2)}{\sqrt{\mathcal{S}_j\mathcal{S}_L}} - \frac{R_o(X_1-Y_1)}{\sqrt{\mathcal{S}_j\mathcal{S}_J}} - \frac{R_o(X_2-Y_2)}{\sqrt{\mathcal{S}_l\mathcal{S}_L}} + \frac{R_o(X_2-Y_1)}{\sqrt{\mathcal{S}_l\mathcal{S}_J}}\right] M_{jlJL}
\end{aligned} \tag{B.2}$$

for $Z > 0$, with the initial condition

$$M_{jlJL} = \delta(X_1 - X_1')\delta(X_2 - X_2')\delta(Y_1 - Y_1')\delta(Y_2 - Y_2') \quad \text{at } Z = 0. \tag{B.3}$$

Let us consider the case $j = l$, $J = L$, $\omega_1 = \omega_2 = \omega$, and $\omega_3 = \omega_4 = \omega'$. These moments M_{jjJJ} are needed in section 8 to show the statistical stability of the time reversal function in the case of an array that spans the entire depth of the waveguide.

We look for the fourth-order moment for $X_1 = X_2$ and $Y_1 = Y_2$ in the support of the array. So we parameterize

$$X_1 = |A_X|\xi + X_{d,j}(\omega)\frac{u}{2}, \quad X_2 = |A_X|\xi - X_{d,j}(\omega)\frac{u}{2}, \tag{B.4}$$

$$X_1' = |A_X|\xi' + X_{d,j}(\omega)\frac{u'}{2}, \quad X_2' = |A_X|\xi' - X_{d,j}(\omega)\frac{u'}{2}, \tag{B.5}$$

$$Y_1 = |A_X|\zeta + X_{d,J}(\omega')\frac{v}{2}, \quad Y_2 = |A_X|\zeta - X_{d,J}(\omega')\frac{v}{2}, \tag{B.6}$$

$$Y_1' = |A_X|\zeta' + X_{d,J}(\omega')\frac{v'}{2}, \quad Y_2' = |A_X|\zeta' - X_{d,J}(\omega')\frac{v'}{2}. \tag{B.7}$$

Equation (B.2) becomes (remember $C_o''(0) = 1/\ell^2$)

$$\partial_Z M_{jjJJ} \approx \left[\frac{i}{\beta_j X_{d,j}|A_X|}\partial_\xi\partial_u + \frac{i}{\beta_J X_{d,J}|A_X|}\partial_\zeta\partial_v - \frac{X_{d,j}^2 u^2}{\ell^2\mathcal{S}_j} - \frac{X_{d,J}^2 v^2}{\ell^2\mathcal{S}_J} - \frac{2X_{d,j}X_{d,J}uvC_o''[|A_X|(\xi-\zeta)]}{\sqrt{\mathcal{S}_j\mathcal{S}_J}}\right] M_{jjJJ}, \tag{B.8}$$

with the initial condition

$$M_{jjJJ} = \frac{1}{X_{d,j}X_{d,j}|A_X|^2}\delta(u-u')\delta(\xi-\xi')\delta(v-v')\delta(\zeta-\zeta') \qquad \text{at } Z = 0. \tag{B.9}$$

We address two cases.

Case 1. The array diameter $|A_X|$ is much larger than ℓ. This allows us to simplify (B.8) as

$$\partial_Z M_{jjJJ} \approx \left[\frac{i}{\beta_j X_{d,j}|A_X|}\partial_\xi\partial_u + \frac{i}{\beta_J X_{d,J}|A_X|}\partial_\zeta\partial_v - \frac{X_{d,j}^2 u^2}{\ell^2\mathcal{S}_j} - \frac{X_{d,J}^2 v^2}{\ell^2\mathcal{S}_J}\right] M_{jjJJ}, \tag{B.10}$$

which has a separable form in (u,ξ) and (v,ζ), and we get (following the same method as in the case of second-order moments)

$$M_{jjJJ} \approx \frac{\beta_j\beta_J}{4\pi^2Z^2}\exp\left[-\frac{i\beta_j X_{d,j}|A_X|(\xi-\xi')(u-u')}{Z} - \frac{i\beta_J X_{d,J}|A_X|(\zeta-\zeta')(v-v')}{Z}\right]$$
$$\times\exp\left\{-\frac{Z}{3\ell^2}\left[\frac{X_{d,j}^2(u^2+u'^2+uu')}{\mathcal{S}_j} + \frac{X_{d,J}^2(v^2+v'^2+vv')}{\mathcal{S}_J}\right]\right\}. \tag{B.11}$$

Equivalently, in terms of the original variables,

$$M_{jjJJ} \approx \frac{\beta_j\beta_J}{4\pi^2Z^2}$$
$$\times\exp\left[-\frac{i\beta_j[(X_1-X_1')^2-(X_2-X_2')^2]}{2Z} - \frac{i\beta_J[(Y_1-Y_1')^2-(Y_2-Y_2')^2]}{2Z}\right]$$
$$\times\exp\left[-\frac{1}{2}\frac{(X_1-X_2)^2+(X_1'-X_2')^2+(X_1-X_2)(X_1'-X_2')}{X_{d,j}^2}\right]$$
$$\times\exp\left[-\frac{1}{2}\frac{(Y_1-Y_2)^2+(Y_1'-Y_2')^2+(Y_1-Y_2)(Y_1'-Y_2')}{X_{d,J}^2}\right], \tag{B.12}$$

which is equal to $\mathbb{E}\left[\mathcal{T}_j\overline{\mathcal{T}_j}\right]\mathbb{E}\left[\mathcal{T}_J\overline{\mathcal{T}_J}\right]$.

Case 2. The array diameter $|A_X|$ is smaller than ℓ. Then (B.2) becomes

$$\begin{aligned}\partial_Z M_{jjJJ} \approx \Big[&\frac{i}{\beta_j X_{d,j}|A_X|}\partial_\xi\partial_u + \frac{i}{\beta_J X_{d,J}|A_X|}\partial_\zeta\partial_v \\ &- \frac{X_{d,j}^2u^2}{\ell^2\mathcal{S}_j} - \frac{X_{d,J}^2v^2}{\ell^2\mathcal{S}_J} - \frac{2X_{d,j}X_{d,J}uv}{\ell\sqrt{\mathcal{S}_j\mathcal{S}_J}}\Big]M_{jjJJ},\end{aligned} \tag{B.13}$$

with the initial condition (B.9). This equation can be solved explicitly after Fourier transforming in ξ and ζ. If we let

$$\widehat{M}_{jjJJ} = \int d\xi \int d\zeta M_{jjJJ}e^{iK_\xi\xi+iK_\zeta\zeta}, \tag{B.14}$$

then we have

$$\left[\partial_Z + \frac{K_\xi}{\beta_j X_{d,j}|A_X|}\partial_u + \frac{K_\zeta}{\beta_J X_{d,J}|A_X|}\partial_v\right]\widehat{M}_{jjJJ} \approx -\left(\frac{X_{d,j}u}{\ell\sqrt{\mathcal{S}_j}} + \frac{X_{d,J}v}{\ell\sqrt{\mathcal{S}_J}}\right)^2\widehat{M}_{jjJJ} \tag{B.15}$$

for $Z > 0$ and

$$\widehat{M}_{jjJJ} = \frac{1}{X_{d,j}X_{d,j}|A_X|^2}\delta(u-u')\delta(v-v')e^{iK_\xi\xi'+iK_\zeta\zeta'} \qquad \text{at } \ Z = 0. \tag{B.16}$$

The solution is given by the method of characteristics

$$\begin{aligned}\widehat{M}_{jjJJ} \approx{}& \delta\left(u-u'-\frac{K_\xi Z}{\beta_j X_{d,j}|A_X|}\right)\delta\left(v-v'-\frac{K_\zeta Z}{\beta_J X_{d,J}|A_X|}\right) \\ &\times\exp\left[-\frac{Z^3}{3\ell^2}\left(\frac{K_\xi}{\beta_j\sqrt{\mathcal{S}_j}|A_X|}+\frac{K_\zeta}{\beta_J\sqrt{\mathcal{S}_J}|A_X|}\right)^2\right. \\ &\left.-\frac{Z^2}{\ell^2}\left(\frac{K_\xi}{\beta_j\sqrt{\mathcal{S}_j}|A_X|}+\frac{K_\zeta}{\beta_J\sqrt{\mathcal{S}_J}|A_X|}\right)\left(\frac{X_{d,j}u'}{\sqrt{\mathcal{S}_j}}+\frac{X_{d,J}v'}{\sqrt{\mathcal{S}_J}}\right)-\frac{Z}{\ell^2}\left(\frac{X_{d,j}u'}{\sqrt{\mathcal{S}_j}}+\frac{X_{d,J}v'}{\sqrt{\mathcal{S}_J}}\right)^2\right],\end{aligned} \tag{B.17}$$

and the moment estimate follows from the inverse Fourier transform,

$$\begin{aligned}M_{jjJJ} \approx{}& \frac{\beta_j\beta_J}{4\pi^2Z^2} \\ &\times\exp\left[-\frac{i\beta_j|A_X|X_{d,j}(\xi-\xi')(u-u')}{Z}-\frac{i\beta_J|A_X|X_{d,J}(\zeta-\zeta')(v-v')}{Z}\right] \\ &\times\exp\left\{-\frac{Z}{3\ell^2}\left[\left(\frac{uX_{d,j}}{\sqrt{\mathcal{S}_j}}+\frac{vX_{d,J}}{\sqrt{\mathcal{S}_J}}\right)^2+\left(\frac{u'X_{d,j}}{\sqrt{\mathcal{S}_j}}+\frac{v'X_{d,J}}{\sqrt{\mathcal{S}_J}}\right)^2+\left(\frac{uX_{d,j}}{\sqrt{\mathcal{S}_j}}+\frac{vX_{d,J}}{\sqrt{\mathcal{S}_J}}\right)\left(\frac{u'X_{d,j}}{\sqrt{\mathcal{S}_j}}+\frac{v'X_{d,J}}{\sqrt{\mathcal{S}_J}}\right)\right]\right\}.\end{aligned}$$

Equivalently, in terms of the original variables,

$$\begin{aligned}M_{jjJJ} \approx{}& \frac{\beta_j\beta_J}{4\pi^2Z^2}\exp\left[-\frac{i\beta_j[(X_1-X_1')^2-(X_2-X_2')^2]}{2Z}-\frac{i\beta_J[(Y_1-Y_1')^2-(Y_2-Y_2')^2]}{2Z}\right] \\ &\times\exp\left[-\frac{1}{2}\left(\frac{X_1-X_2}{X_{d,j}}+\frac{Y_1-Y_2}{X_{d,J}}\right)^2-\frac{1}{2}\left(\frac{X_1'-X_2'}{X_{d,j}}+\frac{Y_1'-Y_2'}{X_{d,J}}\right)^2\right. \\ &\left.-\frac{1}{2}\left(\frac{X_1-X_2}{X_{d,j}}+\frac{Y_1-Y_2}{X_{d,J}}\right)\left(\frac{X_1'-X_2'}{X_{d,j}}+\frac{Y_1'-Y_2'}{X_{d,J}}\right)\right].\end{aligned} \tag{B.18}$$

If $X_1 = X_2$ and $Y_1 = Y_2$, then

$$M_{jjJJ} \approx \frac{\beta_j \beta_J}{4\pi^2 Z^2} \exp\left[-\frac{i\beta_j[(X_1 - X_1')^2 - (X_2 - X_2')^2]}{2Z} - \frac{i\beta_J[(Y_1 - Y_1')^2 - (Y_2 - Y_2')^2]}{2Z} \right] \times \exp\left[-\frac{1}{2}\left(\frac{X_1' - X_2'}{X_{d,j}} + \frac{Y_1' - Y_2'}{X_{d,J}} \right)^2 \right],$$

while

$$\mathbb{E}\left[\mathcal{T}_j \overline{\mathcal{T}_j}\right] \mathbb{E}\left[\mathcal{T}_J \overline{\mathcal{T}_J}\right] \approx \frac{\beta_j \beta_J}{4\pi^2 Z^2} \exp\left[-\frac{i\beta_j[(X_1 - X_1')^2 - (X_2 - X_2')^2]}{2Z} - \frac{i\beta_J[(Y_1 - Y_1')^2 - (Y_2 - Y_2')^2]}{2Z} \right] \times \exp\left[-\frac{1}{2}\left(\frac{(X_1' - X_2')^2}{X_{d,j}^2} + \frac{(Y_1' - Y_2')^2}{X_{d,J}^2} \right) \right].$$

Here we can see that the fourth-order moment is not equal to the product of the second-order moments.

REFERENCES

[1] R. Alonso, L. Borcea, and J. Garnier, *Wave propagation in waveguides with random boundaries*, Commun. Math. Sci., 11 (2012), pp. 233–267.

[2] G. Bal and L. Ryzhik, *Time reversal and refocusing in random media*, SIAM J. Appl. Math., 63 (2003), pp. 1475–1498.

[3] P. Blomgren, H. Zhao, and G. Papanicolaou, *Super-resolution in time-reversal acoustics*, J. Acoust. Soc. Am., 111 (2002), pp. 230–248.

[4] L. Borcea, J. Garnier, G. Papanicolaou, and C. Tsogka, *Enhanced statistical stability in coherent interferometric imaging*, Inverse Problems, 27 (2011), 085003.

[5] L. Borcea, G. Papanicolaou, and C. Tsogka, *Adaptive interferometric imaging in clutter and optimal illumination*, Inverse Problems, 22 (2006), pp. 1405–1436.

[6] L. Borcea, G. Papanicolaou, and C. Tsogka, *Asymptotics for the space-time Wigner transform with applications to imaging*, in Stochastic Differential Equations: Theory and Applications, Interdiscipl. Math. Sci. 2, P. H. Baxendale and S. V. Lototsky, eds., World Scientific, Hackensack, NJ, 2007, pp. 91–111.

[7] L. Borcea, G. Papanicolaou, and C. Tsogka, *Interferometric array imaging in clutter*, Inverse Problems 21 (2005), pp. 1419–1460.

[8] L. B. Dozier and F. D. Tappert, *Statistics of normal mode amplitudes in a random ocean. I. Theory*, J. Acoust. Soc. Am., 63 (1978), pp. 353–365.

[9] A. Fannjiang, *White-noise and geometrical optics limits of Wigner-Moyal equation for wave beams in turbulent media* II. *Two-frequency Wigner distribution formulation*, J. Statist. Phys., 120 (2005), pp. 543–586.

[10] M. Fink, *Time reversed acoustics*, Phys. Today, 20 (1997), pp. 34–40.

[11] J.-P. Fouque, J. Garnier, G. Papanicolaou, and K. Sølna, *Wave Propagation and Time Reversal in Randomly Layered Media*, Springer, New York, 2007.

[12] J. Garnier and G. Papanicolaou, *Pulse propagation and time reversal in random waveguides*, SIAM J. Appl. Math., 67 (2007), pp. 1718–1739.

[13] C. Gomez, *Wave propagation in shallow-water acoustic random waveguides*, Commun. Math. Sci., 9 (2011), pp. 81–125.

[14] C. Gomez, *Wave Propagation in Shallow-Water Acoustic Waveguides with Rough Boundaries*, preprint, arXiv:0911.5646 [math.PR], submitted.

[15] W. Kohler and G. Papanicolaou, *Wave propagation in a randomly inhomogeneous ocean*, in Wave Propagation and Underwater Acoustics, Lecture Notes in Phys. 70, J. B. Keller and J. S. Papadakis, eds., Springer-Verlag, Berlin, 1977, pp. 153–223.

[16] W. A. Kuperman, W. S. Hodkiss, H. C. Song, T. Akal, C. Ferla, and D. R. Jackson, *Experimental demonstration of an acoustic time-reversal mirror*, J. Acoust. Soc. Am., 103 (1998), pp. 25–40.

[17] H. J. Kushner, *Approximation and Weak Convergence Methods for Random Processes*, MIT Press, Cambridge, MA, 1984.

[18] G. Papanicolaou and W. Kohler, *Asymptotic theory of mixing stochastic differential equations*, Comm. Pure Appl. Math., 27 (1974), pp. 641–668.

[19] G. Papanicolaou and W. Kohler, *Asymptotic analysis of deterministic and stochastic equations with rapidly varying components*, Comm. Math. Phys., 45 (1975), pp. 217–232.
[20] G. Papanicolaou, L. Ryzhik, and K. Sølna, *Self-averaging from lateral diversity in the Itô–Schrödinger equation*, Multiscale Model. Simul., 6 (2007), pp. 468–492.
[21] J. Weidmann, *Spectral Theory of Ordinary Differential Operators*, Lecture Notes in Math. 1258, Springer-Verlag, Heidelberg, 1987.